

Rare-earth polarized absorption spectra as a structural tool

Mattias Klintonberg

*Uppsala University, The Ångström Laboratory,
Box 538, S-751 21 UPPSALA, Sweden*

Summer, 1997

PhD Thesis

Dissertation for the Degree of Doctor of Philosophy in Solid State Physics presented at Uppsala University in 1997

Abstract

Klintonberg, M. 1997. Rare-Earth Polarized Absorption Spectra as a Structural Tool. Acta Universitatis Upsaliensis. *Comprehensive Summaries of Uppsala Dissertations from the Faculty of Science and Technology* 313. 54 pp. Uppsala. ISBN 91-554-4054-1.

The theoretical framework has been built for the subsequent use of rare-earth polarized absorption spectra to provide direct structural information.

The technique developed earlier for simulating the polarized absorption spectrum of rare-earth ions in various solid/liquid/amorphous materials has been improved. A refinement of Judd/Ofelt theory has been used to simulate the polarized oscillator strengths between Stark levels for rare-earths in a number of compounds. The experimental agreement is generally good both for σ - and π -polarization. For optically isotropic compounds, the polarization average agrees well with experiment.

The energy matrix has been constructed using a standard Hamiltonian. The 364×364 energy matrices (for Nd^{3+} and Er^{3+}) are diagonalized directly. The crystal field has then been calculated using an electrostatic multipole expansion of the rare-earth environment. Charge neutrality and self consistent dipoles were achieved while the quadrupole contributions were considered without achieving self consistency.

The molecular dynamics simulation technique has then been used to generate a number of physically representative environments for the rare-earth ions. This has made it possible, for example, to study the intensity contributions from rare-earth ions situated at centres of inversion. These have been shown to be non-negligible for some transitions.

It has also been shown that configuration interaction (CI) effects are crucial for a successful simulation of rare-earth polarized absorption spectra. The CI parameters, fitted to reproduce experimental energy levels, have been shown to improve the eigenvectors.

A scheme for simulating polarized emission spectra and an assessment of the usefulness of the method as a structural probe are also presented.

Key words: rare earth, polarized oscillator strength, molecular dynamics, crystal field.

Mattias Klintonberg, Inorganic Chemistry, The Ångström Laboratory, Uppsala University, Box 538, S-751 21 UPPSALA, Sweden

© Mattias Klintonberg 1997

ISSN 1104-232X

ISBN 91-554-4054-1

Printed in Sweden by Eklundshofs Grafiska AB, Uppsala 1997

To

Rebecka

This thesis is based on the following papers:

- I. Use of Polarized Optical Absorption to Obtain Structural Information for $\text{Na}^+/\text{Nd}^{3+}$ β'' -Alumina
S. Edvardsson, M. Klintenberg and J. O. Thomas
Phys. Rev. B **54**, 17476 (1996).
- II. Calculation of Energy Levels and Polarized Oscillator Strengths for $\text{Nd}^{3+}:\text{YAG}$
M. Klintenberg, S. Edvardsson and J. O. Thomas
Phys. Rev. B **55**, 10369 (1997).
- III. Role of the Electrostatic Model in Calculating Rare-Earth Crystal-Field Parameters
S. Edvardsson and M. Klintenberg
Submitted to J. Alloys Comp.
- IV. Effect of Configuration Interaction on Calculated Polarized UV-VIS Absorption Spectra: A Molecular Dynamics Based Study
M. Klintenberg and J. O. Thomas
Phys. Rev. B. Accepted for publication (scheduled for the issue B15 15Nov97).
- V. Energy Level and Polarized Oscillator Strength Calculation for $\text{Er}^{3+}:\text{Y}_2\text{O}_3$:
A Molecular Dynamics Based Study
M. Klintenberg, S. Edvardsson and J. O. Thomas
Submitted to J. Alloys Comp.

Other papers:

- VI. Oscillator Strength Calculation for Nd_2O_3 and $\text{Nd}^{3+}:\text{LiYF}_4$
M. Klintenberg, S. Edvardsson and J. O. Thomas
J. Lumin. **72-74**, 218 (1997).
- VII. Determining Point Charges that Accurately Reproduce Crystal Fields for *ab initio* Molecular Cluster Calculations
S. E. Derenzo, M. Klintenberg and M. J. Weber
In Manuscript.

Contents

1	Introduction	1
2	Group theory and classification of states	5
2.1	Introduction	5
2.2	Lie groups	6
2.3	The coefficients of fractional parentage (CFP)	9
3	The energy matrix	11
3.1	The Hamiltonian	11
3.1.1	The coulomb interaction (H_{EL})	11
3.1.2	The spin-orbit interaction (H_{SO})	13
3.1.3	The crystal field interaction (H_{CF})	13
3.1.4	Configuration interaction (H_{CIL} , H_{CINL}) and other interactions . . .	14
3.2	The radial wave functions	16
3.3	The crystal field parameters ($A_q^{(k)}$)	17
3.4	Diagonalization and numerical detail	18
4	The oscillator strengths; absorption/emission spectra	21
4.1	Introduction	21
4.2	Judd-Ofelt theory and refinements	21
4.2.1	The inhomogeneous dielectric mechanism	23
4.2.2	Other effects	23
4.3	Absorption/emission spectra	24
4.4	Results	24
5	Molecular dynamics simulation	29
5.1	Introduction	29
5.2	The theory	29
5.3	Results	30
6	A structural probe, materials design, laser properties	33
7	Brief summary of results and concluding remarks	37
A	Some useful relations	39
A.1	Miscellaneous	39
A.2	$n - j$ symbols	39

B An alternative scheme; the seniority number	41
C The coefficients of fractional parentage for f^3	43
D The metric tensor and Casimir's operator	45
Summary of the papers	47
Acknowledgements	49
Bibliography	50

Chapter 1

Introduction

The first rare earth (cerium) was discovered in 1803. The remainder of the elements of the rare-earth series were identified over the next 110 years. Sweden, and more specifically the village of Ytterby (near Vaxholm) in Stockholm's archipelago, has played an important role in the history of rare-earths since many of them were first discovered there, e.g. gadolinium (named after Professor Johan Gadolin), holmium (latin for Stockholm), thulium (Thule is an old word for the Nordic countries) and, of course, ytterbium, erbium, terbium and yttrium; all were named after Ytterby itself.

The discoverers of the rare earths could never have imagined the variety of different areas of application these elements would find. Optical, opto-electronic, magnetic and high-temperature superconductors are just some examples. Amongst these, optical applications are probably the most far-reaching, ranging from inorganic solid lasers, to scintillators, windows and optical fibres. Neodymium (Nd^{3+}) ions are probably the most commonly used solid-state laser ions, with examples such as $\text{Nd}^{3+}:\text{YAG}$ and $\text{Nd}^{3+}:\text{LiYF}_4$, while erbium (Er^{3+}) is used in optical fibres since a minimum in the optical attenuation occurs at $1.6 \mu\text{m}$. The many well-defined energy levels within the $4f$ shell make the rare-earth ions ideal as laser ions because of the many possible laser channels. Up-conversion is also possible, in which two or more lower-energy photons are used to excite a higher energy state, resulting in emission at an energy higher than that used for the pumping. For extensive reviews of rare-earth applications, see Weber [1] and Kaminskii [2].

The calculation of an absorption/emission spectrum for a rare-earth ion in some solid/liquid/amorphous host material involves solving the Schrödinger equation, i.e. determining the eigenvalues and eigenstates for the system. In the work reported in this thesis, only the rare-earth ions have been treated by quantum mechanical methods, thus greatly reducing the size of the calculation. The crystal field (CF) experienced by the ions is expressed as an electrostatic multipole expansion, using contributions from mono-, di- and quadrupole moments. The dipole moments have been calculated self consistently. Some might argue that the electrostatic model is a gross oversimplification but, as will be shown, the motion of the rare-earth ions and their neighbours introduce uncertainties in the CF parameters. It is therefore reasonable to fully explore the result of using an electrostatic model.

Chapter 2 deals with the problem of labelling l^n states or, in this case, $4f^n$ states. This was treated by Racah in the 1940's in his four classic papers [3–6]. His first paper gives a closed formula which replaces the so-called "diagonal sum method" (developed by Slater [7]) for calculating the energy levels in two electron systems. In a second paper [4], he defines the tensor operator and develops the appropriate tensor algebra (used throughout this thesis).

The fractional parentage coefficients were introduced in his third paper [5] and, in a fourth paper, he uses group theory to label states and calculate the energy matrices [6]. The chapter also gives a very brief introduction to Lie algebra and discusses the various groups of interest for labelling l^n states.

In Chapter 3, the methods used for evaluating the different matrix elements are described. Perturbation theory is used, with the totally degenerated $4f^n$ state (resulting from the central field approximation) being taken as a starting point. Perturbation theory is indeed valid for the rare-earth ions, since the $4f^n$ shell is primarily screened by the outer $5s$ and $5p$ shells. Starting with the Coulomb interaction, the formalism used will be described up to the different configuration interactions, which are included *via* second-order perturbation theory. Chapter 3 deals also with the radial wavefunctions, and a presentation is made of the methods used for handling the crystal field at each time step in the molecular dynamics (MD) simulation. Some comments on numerical issues are also made.

Chapter 4 outlines the polarized oscillator strength calculations and the different mechanisms involved. The theory for the polarized Stark-Stark level transitions is based on the well known Judd/Ofelt theory [8,9], which is a highly successful quantitative theory for calculating unpolarized oscillator strengths between J -manifolds. The electric dipole transitions are not parity-allowed, since the dipole operator is odd and therefore does not commute with the parity operator π .¹ However, Judd and Ofelt showed that the crystal field mixes-in a small portion of odd parity wavefunctions, thus allowing the (albeit small) electric dipole transition. The inhomogeneous dielectric mechanism is also outlined. A short section at the end of Chapter 4 concerns the differences, within this model, between absorption and emission spectra. The last pages of Chapter 4 present some of the results.

Chapter 5 describes the molecular dynamics (MD) simulation technique used to simulate the thermally induced fluctuations of the ions. Some results are presented. The importance of using MD or Monte-Carlo techniques to calculate the polarized oscillator strengths is emphasized.

A discussion of the potential use of the simulation technique is given in Chapter 6, and a brief summary of the results obtained in Chapter 7.

The various expressions that appear in this thesis are not derived rigorously, but in a somewhat sketchy manner; for a more complete treatment, the reader is referred to the original work of Racah, Rajnak, Wybourne, Judd and others. The advent of powerful computer facilities has meant that “simulation” can now be added to the two main areas: theory and experiment. It is to this new area that the work belongs, although much effort has also been made in the theoretical aspects of rare-earth optics.

Figure 1.1 gives a flow chart for the simulation technique used for calculating a polarized absorption/emission spectrum, as developed in this thesis. The content of the boxes in the flow chart will be explained in the thesis. Starting from some experimental structure (or from a trial structure if relevant), appropriate molecular dynamics potentials are derived. It is then a straightforward matter to run an MD simulation to generate a number of physically representative environments for the rare-earth ions. These different environments are essential for a valid simulation of the crystal-field, and for the subsequent crystal field parameter calculation. The radial wavefunctions must also be calculated so that the shielding parameters (σ_k), the radial integrals $\langle r^k \rangle$, and the different polarizabilities ($\alpha^{(1)}$, $\alpha^{(2)}$) can be calculated.

The energy matrix can then be constructed and diagonalized, to get the eigenvectors

¹Since most Physics is hermitian, it follows that $\pi^\dagger r \pi = -r$, which is equivalent to $[r, \pi] = -2\pi r \neq 0$.

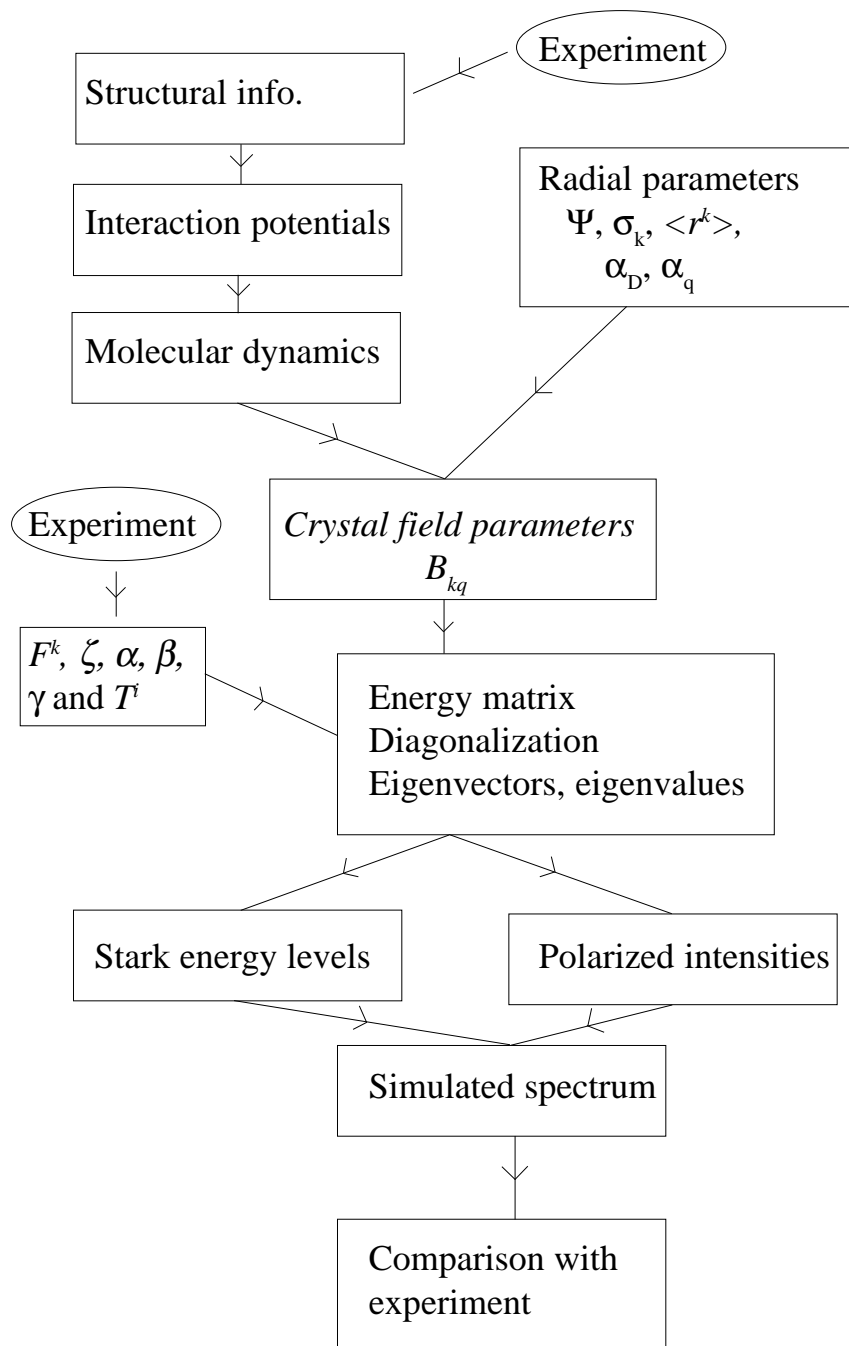


Figure 1.1: Flow chart for the simulation of a polarized absorption/emission spectrum.

and the eigenvalues (Stark energy levels) for the system. These are then used to construct a polarized absorption/emission spectrum.

A large portion of the thesis is devoted to the labelling of states and the construction of the energy matrix. This explains the often technical and sometimes tedious sections in some of the chapters. A number of texts and textbooks of atomic physics, quantum mechanics, spectroscopy and general physics have been consulted throughout the work; these are listed as references [10–31].

Chapter 2

Group theory and classification of states

2.1 Introduction

The use of group theory and tensor operator techniques in spectroscopy have been treated rigorously by Racah [3–6, 32] and Judd [31]. Only a brief overview is provided here to give some background to the quantum numbers and coefficients of fractional parentage (CFP) used.

It is well known that the Schrödinger equation is not solvable for most many-body problems. Perturbation theory must therefore be used to calculate the energy levels and eigenvectors for a f^n system. The central-field approximation is used to find the zeroth-order eigenvector (ground-state) on which to base the perturbation theory. In this approximation, the field from the nucleus (infinite mass point charge) and the mean field from all independently moving electrons in the system (57 in the case of Nd^{3+}) are superimposed. The approximate solutions to the Schrödinger equation can thus be written in the form:

$$\psi(r\theta\phi) = r^{-1}R_{nl}(r)Y_{lm_l}(\theta\phi) \quad (2.1)$$

since the resulting potential is spherically symmetric. At this stage, the energy levels characterized by the quantum numbers (nl) are highly degenerate. Once again, taking Nd^{3+} as an example, the unfilled $4f^3$ configuration can be 364-fold degenerate. The degeneracy is lifted by various Hamiltonians. Eq. (2.1) will be the starting point for the application of perturbation theory. Since we are only interested in the eigenstates and eigenvalues of the interior of the $4f^n$ configuration, perturbation operators which move the configuration as a whole can be neglected, i.e. the energy corresponding to the degenerate $4f^n$ configuration is set to zero.

The first perturbing potential is the coulomb interaction (H_{EL}) between the $4f^n$ electrons. The effect of this Hamiltonian is to split the $4f^n$ configuration into terms characterized by the quantum numbers (γSL); S is the total spin angular momentum, L the total orbital angular momentum of the configuration; we shall return to γ a little later; ($SLM_S M_L$) are good quantum numbers since, $[\mathbf{S}_z, H_{EL}] = [\mathbf{S}^2, H_{EL}] = [\mathbf{L}_z, H_{EL}] = [\mathbf{L}^2, H_{EL}] = 0$. The next perturbing potential is the spin-orbit interaction (H_{SO}). H_{SO} splits the terms into multiplets characterized by (γSLJ). Note that the quantization has been changed from $SLM_S M_L$ to $SLJM_J$, since H_{SO} does not commute with \mathbf{S} and \mathbf{L} separately, but with their resultant $\mathbf{J} = \mathbf{S} + \mathbf{L}$; ($\gamma SLJM_J$) are the quantum numbers used throughout and will be the

starting point for the following discussion. Later in this work, further perturbing Hamiltonians will be introduced, such as the crystal field Hamiltonian and the different configuration interaction Hamiltonians.

When performing calculations of the type described above on systems with more than three (or equal) electrons, $(SLJM_J)$ will not specify the states uniquely, i.e. the situation can arise that two states (1,2) have the same quantum number, $(SLJM_J)_1 = (SLJM_J)_2$. This is where γ is introduced to distinguish these states. It is natural to turn to group theory when looking for the quantum numbers (γ), since $(SLM_S M_L)$ have attractive group theoretical properties. For example, the $2L + 1$ ($M_L = -L, \dots, L$) components of a term transform according to the representation (representation matrix) \mathcal{D}_L of the group R_3 when rotated in three-dimensional space. This is natural, since the eigenfunctions of \mathbf{L} (spherical harmonics) are a basis for the representation of the group of all rotations in three-dimensions. (R_3) and (LM_L) can thus be used to label the representation:

$$R(\alpha\beta\gamma)\psi(LM_L) = \sum_{L'M_{L'}} \psi(L'M_{L'})\mathcal{D}_{M_L M_{L'}}^{L'L'}(\alpha\beta\gamma) \quad (2.2)$$

where

$$\mathcal{D}_{M_L M_{L'}}^{L'L'}(\alpha\beta\gamma) = \langle LM_L | R(\alpha\beta\gamma) | L'M_{L'} \rangle \quad (2.3)$$

and

$$R(\alpha\beta\gamma) = e^{-i\alpha L_z} e^{-i\beta L_y} e^{-i\gamma L_z} \quad (2.4)$$

2.2 Lie groups

The application of Lie's theory of continuous groups to the problem of labelling the states has been most successful. Lie showed that, if

$$X_\sigma = u_\sigma^i \frac{\partial}{\partial x^i} \quad (2.5)$$

are the infinitesimal operators of a group, and X_σ satisfy the commutation relations

$$[X_\sigma, X_\rho] = c_{\sigma\rho}^\tau X_\tau, \quad (2.6)$$

the operators

$$1 + \delta a^\sigma X_\sigma \quad (2.7)$$

form a group. The labels of the irreducible representation can then be used as labels of the states. $c_{\sigma\rho}^\tau$ are the structure constants, and these determine the properties of the group. u_σ^i can be seen as a generalized velocity field. This term is better understood when looking at the types of infinitesimal transformation that Lie studied:

$$x^i + dx^i = x^i + \left(\frac{\partial f^i(x^i, a^\sigma)}{\partial a^\sigma} \right)_{a=0} \delta a^\sigma = x^i + u_\sigma^i(x) \delta a^\sigma \quad (2.8)$$

$f^i(x^i, a)$ are the transformations, and a^σ the parameters of the transformation.

The four classic papers of Racah [3–6] introduced the tensor operators which have turned out to be very useful tools in, for example, spectroscopy. He also applied the theory of continuous groups to the problem of labelling states. The irreducible spherical tensor operators of rank k , Racah [4], Eq. (23a) and (23b), are defined as:

$$[(\mathbf{L}_x \pm \mathbf{L}_y), T_q^{(k)}] = \sqrt{(k \mp q)(k \pm q + 1)} T_{q\pm 1}^{(k)} \quad (2.9)$$

$$[\mathbf{L}_z, T_q^{(k)}] = qT_q^{(k)} \quad (2.10)$$

Note that $T_q^{(k)}$ have the same commutation relations as the spherical harmonics. The tensor operators defined in Eq. (2.9) and Eq. (2.10) satisfy commutation relations of the type Eq. (2.6); this will be shown below. As a consequence, the infinitesimal operators of the corresponding group can be used to find the quantum numbers (γ). This is completely analogous to the case of R_3 with the infinitesimal operators \mathbf{L} and the quantum numbers (LM_L). It is indeed true that a group \mathcal{G} can be found which contains R_3 as a subgroup, and that the labels of \mathcal{G} 's irreducible representations can be used as quantum numbers (γ) to label the states. Before identifying these subgroups and irreducible representations, the commutation relation for irreducible tensor operators will be demonstrated. First defining the unit tensor operator from:

$$\langle n'l' || u^{(k)} || nl \rangle = \delta_{n'n} \delta_{l'l} \quad (2.11)$$

Using the Wigner-Eckart theorem Eq. (A.2 in Appendix A), the unit operator Eq. (A.1), the orthogonality relation Eq. (A.5), and the formula for the sum of the products of three $3j$ symbols Eq. (A.7), it can be shown that¹:

$$u_{q_2}^{(k_2)} | lm_l \rangle = \sum_{m'_l} (-1)^{l-m'_l} \begin{pmatrix} l & k_2 & l \\ -m'_l & q_2 & m_l \end{pmatrix} | lm'_l \rangle \quad (2.12)$$

$$\begin{aligned} & u_{q_1}^{(k_1)} u_{q_2}^{(k_2)} | lm_l \rangle \\ &= \sum_{m'_l m''_l} (-1)^{2l-m'_l-m''_l} \begin{pmatrix} l & k_1 & l \\ -m'_l & q_1 & m'_l \end{pmatrix} \begin{pmatrix} l & k_2 & l \\ -m'_l & q_2 & m_l \end{pmatrix} | lm''_l \rangle \\ &= \sum_{m'_l k_3 q_3} (-1)^{3l-m'_l-q_3+k_1+k_2+k_3} [k_3] \begin{Bmatrix} k_1 & k_2 & k_3 \\ l & l & l \end{Bmatrix} \begin{pmatrix} l & k_3 & l \\ -m'_l & q_3 & m_l \end{pmatrix} \\ &\times \begin{pmatrix} k_1 & k_2 & k_3 \\ q_1 & q_2 & -q_3 \end{pmatrix} | lm''_l \rangle \\ &= \sum_{k_3 q_3} [k_3] (-1)^{2l-q_3+k_1+k_2+k_3} \begin{Bmatrix} k_1 & k_2 & k_3 \\ l & l & l \end{Bmatrix} \begin{pmatrix} k_1 & k_2 & k_3 \\ q_1 & q_2 & -q_3 \end{pmatrix} \\ &\times u_{q_3}^{(k_3)} | lm_l \rangle \end{aligned} \quad (2.13)$$

The only difference between $u_{q_1}^{(k_1)} u_{q_2}^{(k_2)} | lm_l \rangle$ and $u_{q_2}^{(k_2)} u_{q_1}^{(k_1)} | lm_l \rangle$ is the phase $(-1)^{k_1+k_2+k_3}$ which originates in the symmetry properties of the $3j$ - symbol; see Eq. (A.8). The commutation relations for irreducible tensor operators thus become:

$$[u_{q_1}^{(k_1)}, u_{q_2}^{(k_2)}] = c_{\sigma\rho}^{\tau} u_{q_3}^{(k_3)} \quad (2.14)$$

with the structure constants [$\sigma = (k_1 q_1)$, $\rho = (k_2 q_2)$ and $\tau = (k_3 q_3)$]:

$$c_{\sigma\rho}^{\tau} = \sum_{k_3 q_3} [k_3] (-1)^{2l-q_3} \{ (-1)^{k_1+k_2+k_3} - 1 \} \begin{Bmatrix} k_1 & k_2 & k_3 \\ l & l & l \end{Bmatrix} \begin{pmatrix} k_1 & k_2 & k_3 \\ q_1 & q_2 & -q_3 \end{pmatrix} \quad (2.15)$$

¹[k]=2k+1

Clearly, Eq. (2.14) has the same structure as Eq. (2.6), and the tensor operators $u_q^{(k)}$ or $U_q^{(k)} = \sum_i (u_q^{(k)})_i$ (the sum runs over all electrons) will therefore serve as the infinitesimal operators of a Lie group, with its properties determined by Eq. (2.15). Analogous to Eq. (2.7), the operators

$$1 + \sum_{kq} \delta a_{kq} U_q^{(k)} \quad (2.16)$$

will form a group in whose irreducible representations we are interested. Notice that the symmetry properties of $6j$ and $3j$ symbols place the following restrictions on k and q : $0 \leq k \leq 2l$ and $-k \leq q \leq k$. By investigating matrix elements of Eq. (2.16) and imposing restrictions on the transformations [Eq. (2.16) in matrix form], Racah [6, 32] and Judd [31] obtained the following succession of groups and subgroups in $2l + 1$ dimensions:

$$GL_{2l+1} \supset U_{2l+1} \supset SU_{2l+1} \supset R_{2l+1} \supset R_3 \quad (2.17)$$

where GL is the full linear group, U is the unitary group, SU is the special unitary group or unimodular group (only transformations with determinant +1 allowed) and R is the rotation group or proper real orthogonal group. In the case of $l = 3$ (f -electrons), yet another subgroup of R_7 could be found, G_2 . The succession of groups and subgroups now becomes:

$$GL_7 \supset U_7 \supset SU_7 \supset R_7 \supset G_2 \supset R_3 \quad (2.18)$$

According to Racah [6], the irreducible representations of R_7 and G_2 , characterized by $W = (w_1 w_2 \dots w_l)$ and $U = (u_1 u_2)$, can be used as the additional quantum numbers [$\gamma = WU = (w_1 w_2 \dots w_l)(u_1 u_2)$]. Table I, given by Judd [31]², shows the quantum numbers for the case of f^3 :

Table I. Quantum numbers for f^3

$[\gamma_1 \gamma_2 \dots \gamma_7]$	$(w_1 w_2 w_3)$	$(u_1 u_2)$	L
[1110000]	(111)	(00)	S
		(10)	F
		(20)	DGI
[2100000]	(100)	(10)	F
		(11)	PH
		(20)	DGI
		(21)	$DFGHL$

$[\gamma_1 \gamma_2 \dots \gamma_7]$ are the irreducible representations of U_7 . These irreducible representations can be dropped, since they are equivalent of specifying (S), and the f^3 (or f^{11}) states are now completely defined by:

$$| f^3(w_1 w_2 w_3)(u_1 u_2) SLJM_J \rangle = | f^3 WUSLJM_J \rangle \quad (2.19)$$

Yet another quantum number (τ) must be added in Eq. (2.19) for the case of $f^{5,6,7,8,9}$ since, for example, $(221)(31)F$ occurs twice. This is seen from Table 5-3 in Judd [31].

²Table I can be constructed from Table 5-1, 5-2 and 5-3 of Judd [31]

2.3 The coefficients of fractional parentage (CFP)

Racah not only applied the theory of continuous groups to the problem of labelling states, he also introduced coefficients of fractional parentage (CFP) in the third of his four papers [5]. Once calculated, these coefficients greatly simplify the work of calculating different matrix elements. Racah's idea was first to couple two equivalent electrons, and then study the effect of adding another electron l to the allowed states (antisymmetric eigenfunctions, $S + L$ even) of l^2 [5]. Three different schemes can be used to add three angular momenta: $(l_1 + l_2) + l_3$ or $l_1 + (l_2 + l_3)$ or $(l_1 + l_3) + l_2$. Changing the schemes for the addition of angular momenta, using Eqs. (3)-(7) of [5], Racah concluded that³:

$$\begin{aligned} |l^2(S'L')lSLM_S M_L \rangle &= \sum_{S''L''} |l, ll(S''L''), SLM_S M_L \rangle \\ &\times \langle l, ll(S''L''), SL | l^2(S'L')lSL \rangle \end{aligned} \quad (2.20)$$

Eq. (2.20) could not be an eigenstate of l^3 since some states would have values of $S'' + L''$ forbidden by the Pauli principle (odd values), and therefore be symmetric. [For the left side of Eq. (2.20), the two electron parts $(l_1 + l_2)$ were constructed to be anti-symmetric since only states with $S' + L'$ even were retained. This is not the case for the two-electron parts $(l_2 + l_3)$ on the right side, since no restrictions are placed on $S'' + L''$; $S'' + L''$ could therefore be odd]. However, a linear combination of Eq. (2.20)

$$|l^3\gamma SLM_S M_L \rangle = \sum_{S'L'} |l^2(S'L')lSLM_S M_L \rangle \langle l^2(S'L')lSL | l^3\gamma SL \rangle \quad (2.21)$$

with vanishing coefficients ($\langle l^2(S'L')lSL | l^3\gamma SL \rangle$) for $S'' + L''$ odd solves this problem. It is then straightforward to decouple the third electron from the ket on the left side of Eq. (2.21). With Eq. (1) of [5], we obtain:

$$\begin{aligned} |l^3\gamma SLM_S M_L \rangle &= \sum_{S'L'M'_S M'_L m_s m_l} |l^2 S' L' M'_S M'_L \rangle |slm_s m_l \rangle \\ &\times \begin{pmatrix} S' & s & S \\ M'_S & m_s & S \end{pmatrix} \begin{pmatrix} L' & l & L \\ M'_L & m_l & L \end{pmatrix} \langle l^2(S'L')lSL | l^3\gamma SL \rangle \end{aligned} \quad (2.22)$$

This equation will be shown to be very useful in calculating different one-particle operator matrix elements. Eq. (2.20) in Eq. (2.21) gives the following equation for the coefficients when $S'' + L''$ is odd:

$$\sum_{S'L'} \langle l, ll(S''L''), SL | l^2(S'L')lSL \rangle \langle l^2(S'L')lSL | l^3\gamma SL \rangle = 0 \quad (2.23)$$

Eq. (2.23) can be used when calculating the CFP's for l^3 . An equation corresponding to Eq. (2.21) can thus be formulated for the case of l^n :

$$\begin{aligned} |l^n\gamma SLM_S M_L \rangle &= \sum_{\gamma' S' L'} |l^{n-1}(\gamma' S' L')lSLM_S M_L \rangle \\ &\times \langle l^{n-1}(\gamma' S' L')lSL | l^n\gamma SL \rangle \\ &= \sum_{\gamma' S' L' \gamma'' S'' L''} |l^{n-2}(\gamma'' S'' L'')l(S'L')lSLM_S M_L \rangle \\ &\times \langle l^{n-2}(\gamma'' S'' L'')lS'L' | l^{n-1}\gamma' S' L' \rangle \\ &\times \langle l^{n-1}(\gamma' S' L')lSL | l^n\gamma SL \rangle \end{aligned} \quad (2.24)$$

³Hereafter, the quantum numbers $M_S M_L$ will be omitted when of no importance.

It is not necessary to proceed further in the recursion relation Eq. (2.24) when using one- and two-particle operators. Three-particle operators (operating in the same space) can be dealt with by using other methods, as will be shown below [Eq. (3.24)]. Note that (γ) in Eq. (2.24) also includes (τ) for the reasons mentioned above.

For the explicit evaluation of the CFP in the case of $4f^3$, see Appendix C.

Chapter 3

The energy matrix

3.1 The Hamiltonian

This chapter will deal with the construction of the energy matrix and the evaluation of the different matrix elements used in papers **II**, **IV**, **V** and **VI**. In paper **I**, the energy matrix was constructed without the use of CFP, making this process excessively tedious. Neither was a complete matrix constructed; only a small part of it (*jj*-mixing and *L, S* mixing were known to be small for the levels studied there). CI effects were introduced in paper **IV**.

As indicated in the preceding chapter, perturbation theory is the technique used to approximately solve the Schrödinger equation. It was found that, as a result of the central field approximation, Eq. (2.1) can be used as the completely degenerate starting point for perturbation theory. In Eq. (2.1), the radial and angular parts are separated, implying that the radial and angular matrix elements can be calculated separately. The Hamiltonian used throughout the calculations is written:

$$H = H_0 + H_{EL} + H_{SO} + H_{CF} + H_{CIL} + H_{CINL} \quad (3.1)$$

where H_0 is a spherical symmetric interaction and can therefore be omitted since it only shifts the whole configuration; H_{EL} is the coulomb interaction; H_{SO} is the spin-orbit interaction; and H_{CF} is the crystal field interaction responsible for the majority of the interesting phenomena discussed in this thesis. H_{CIL} represents linear configuration interaction effects associated with two-particle interaction terms; and H_{CINL} non-linear configuration interaction effects associated with three-particle interaction terms.

3.1.1 The coulomb interaction (H_{EL})

The coulomb interaction between $4f$ electrons is described by ($e = 1$)¹:

$$\begin{aligned} H_{EL} &= \sum_{i < j} \frac{1}{r_{ij}} = \sum_{i < j} \sum_k \frac{r_{<}^k}{r_{>}^{k+1}} P^{(k)}(\cos \theta_{ij}) \\ &= \sum_{i < j} \sum_k \frac{r_{<}^k}{r_{>}^{k+1}} \frac{4\pi}{[k]} \sum_q Y_q^{*(k)}(\theta_i \phi_i) Y_q^{(k)}(\theta_j \phi_j) \\ &= \sum_{i < j} \sum_k \frac{r_{<}^k}{r_{>}^{k+1}} \sum_q (-1)^q (C_{-q}^{(k)})_i (C_q^{(k)})_j \end{aligned}$$

¹Atomic units will be used throughout.

$$= \sum_{i < j} \sum_k \frac{r_{<}^k}{r_{>}^{k+1}} (C_i^{(k)} \cdot C_j^{(k)}) \quad (3.2)$$

where $1/|r_i - r_j|$ has been expanded in Legendre polynomials of $\cos \theta_{ij}$ and the spherical harmonic addition theorem has been applied. Eq. (3.2) can be expressed in a slightly more convenient form (for $4f$ matrix elements) using Eq. (2.11) and Eq. (A.2):

$$H_{EL} = \sum_{i < j} \sum_k \frac{r_{<}^k}{r_{>}^{k+1}} (u_i^{(k)} \cdot u_j^{(k)}) |\langle f || C^{(k)} || f \rangle|^2 \quad (3.3)$$

Note that Eq. (3.3) vanish unless $0 \leq k \leq 6$ and k is even ($3-j$ symbol). Eq. (2.1) suggest that the matrix elements of Eq. (3.3) can be written in the form:

$$\langle 4f^n W' U' \tau' S' L' M'_S M'_L | H_{EL} | 4f^n W' U' \tau S L M_S M_L \rangle = \sum_{k=2,4,6} f_k F^k \quad (3.4)$$

since the radial and angular parts have been separated. The reason for excluding $k = 0$ is that this term only shifts the whole configuration. F^k are the well-known Slater integrals:

$$F^k = \int_0^\infty dr R_{4f}^2(r) \int_r^\infty dr' R_{4f}^2(r') \frac{r^k}{r'^{k+1}} \quad (3.5)$$

The angular coefficients f_k can be evaluated by noting that f_k is essentially the matrix element of $(u^{(k)} \cdot u^{(k)})$:²

$$\begin{aligned} f_k &= \sum_{i < j} \langle f^3 W' U' S' L' M'_S M'_L | (u_i^{(k)} \cdot u_j^{(k)}) | f^3 W U S L M_S M_L \rangle \\ &\times |\langle f || C^{(k)} || f \rangle|^2 \\ &= 6 \sum_{\bar{S}\bar{L}} \langle f^3 W' U' S' L' \{ | f^2(\bar{S}\bar{L}) f W' U' S' L' \rangle \langle f^2(\bar{S}\bar{L}) f W U S L | \} f^3 W U S L \rangle \\ &\times \frac{\delta_{L'L} \delta_{M'_L M_L}}{\sqrt{[L]}} (-1)^{\bar{L}+f+L+0} \sqrt{[L'] [L]} \begin{Bmatrix} \bar{L} & \bar{L} & 0 \\ L & L' & f \end{Bmatrix} \\ &\times (-1)^{f+f+\bar{L}} \sqrt{\bar{L}} \frac{(-1)^{\bar{L}+L+f}}{\sqrt{[\bar{L}] [L]}} [f]^2 \begin{pmatrix} f & k & f \\ 0 & 0 & 0 \end{pmatrix}^2 \end{aligned} \quad (3.6)$$

where Eq. (2.21), Eq. (A.2) and Eq. (44a), Eq. (38) of Racah [4], and the following equations have been used³:

$$(-1)^{L'-M'_L} \begin{pmatrix} L' & 0 & L \\ -M'_L & 0 & M_L \end{pmatrix} = [L]^{-\frac{1}{2}} \delta_{L'L} \delta_{M'_L M_L} \quad (3.7)$$

$$\begin{Bmatrix} \bar{L} & \bar{L} & 0 \\ L & L' & l \end{Bmatrix} = \frac{(-1)^{\bar{L}+L+l}}{\sqrt{[\bar{L}] [L]}} \quad (3.8)$$

$$\langle l' || C^{(k)} || l \rangle = (-1)^{l'} \sqrt{[l'] [l]} \begin{pmatrix} l' & k & l \\ 0 & 0 & 0 \end{pmatrix} \quad (3.9)$$

²Hereafter, all calculations will be made for the simplest non-trivial configuration: $f^3 (f^{11})$.

³ $\langle L || X^0 || L \rangle = \sqrt{[L]} \langle L M_L | X^0 | L M_L \rangle$

3.1.2 The spin-orbit interaction (H_{SO})

The third term in the Hamiltonian is the spin-orbit interaction term. The well-known form of H_{SO} is obtained by studying the non-relativistic limit of the Dirac equation for an electron in an electromagnetic field. This is done by successively performing three Foldy-Wouthuysen transformations on the Hamiltonian. Each of these canonical transformations is followed by a non-relativistic expansion of the transformed Hamiltonian. Details of this technique can be found in Bjorken and Drell [33]. The spin-orbit operator for a spherically symmetric electrostatic potential becomes:

$$H_{SO} = \zeta \sum_{i=1}^3 \mathbf{s}_i \cdot \mathbf{l}_i \quad (3.10)$$

where ζ is the spin-orbit coupling constant. Rewriting Eq. (3.10) results in the slightly more convenient form:

$$H_{SO} = \zeta \sum_{i=1}^3 (v_i^{(1)} \cdot u_i^{(1)}) \langle s \parallel \mathbf{s} \parallel s \rangle \langle f \parallel \mathbf{l} \parallel f \rangle \quad (3.11)$$

where $v_i^{(1)}$ and $u_i^{(1)}$ act in spin and angular-momentum space, respectively. The matrix elements of H_{SO} cannot be evaluated in the $\gamma SLM_S M_L$ representation since H_{SO} does not commute with \mathbf{S} and \mathbf{L} separately⁴, but with their sum $\mathbf{J} = \mathbf{S} + \mathbf{L}$. In the $\gamma SLJM_J$ representation, the matrix element of Eq. (3.11) becomes:

$$\begin{aligned} & \langle W'U'S'L'J'M'_J | H_{SO} | WUSLJM_J \rangle \quad (3.12) \\ &= \zeta \delta_{J'J} \delta_{M'_J M_J} 3(-1)^{S+L'+J'} \left\{ \begin{matrix} L' & L & 1 \\ S & S' & J' \end{matrix} \right\} \\ & \times \sum_{\bar{S}\bar{L}} \langle f^3 W'U'S'L' \{ | f^2(\bar{S}\bar{L}) f W'U'S'L' \rangle \langle f^2(\bar{S}\bar{L}) f WUSL \} | f^3 WUSL \rangle \\ & \times \sqrt{[S'] [S] [L'] [L]} (-1)^{\bar{S}+s+s'+\bar{L}+f+L'} \left\{ \begin{matrix} s & s & 1 \\ S & S' & \bar{S} \end{matrix} \right\} \left\{ \begin{matrix} f & f & 1 \\ L & L' & \bar{L} \end{matrix} \right\} \\ & \times \sqrt{s(s+1)[s]f(f+1)[f]} \quad (3.13) \end{aligned}$$

where Eq. (38), Eq. (44a) and Eq. (44b) of Racah [4], Eq. (2.21), $\mathbf{s} = \sqrt{s(s+1)(2s+1)}v^{(1)}$ and $\mathbf{l} = \sqrt{l(l+1)(2l+1)}u^{(1)}$ have been used.

3.1.3 The crystal field interaction (H_{CF})

The fourth term in the Hamiltonian is the crystal field interaction term. When rare-earth ions are situated in some solid/liquid/amorphous material, they will experience the effects of the crystal field. The crystal field Hamiltonian can be treated by perturbation theory in considering its effects on the partially filled $4f$ shell, since this shell is screened by the filled outer $5s$ and $5p$ shells. Assuming the validity of Laplace's equation in the region between

⁴This means that S and L are not good quantum numbers and can therefore not be used to label the eigenstates, i.e a solution to the Schrödinger equation cannot be found in this representation.

the ions, i.e. no radial overlap, the crystal field potential can be expressed in a multipole expansion. H_{CF} is given by [analogous to Eq. (3.2)]:

$$H_{CF} = \int dr' \frac{\rho(r')}{|r-r'|} = \sum_{kq} A_q^{*(k)} \sum_i r_i^k u_q^{(k)} \langle f || C^{(k)}(\hat{r}_i) || f \rangle \quad (3.14)$$

where $A_q^{(k)}$ are the crystal field parameters, given by:

$$A_q^{(k)} = \int dr' \frac{\rho(r') C_q^{(k)}(\hat{r}')}{r'^{k+1}} \quad (3.15)$$

The different physical environments experienced by the rare-earth ions are characterized through the crystal field parameters $A_q^{(k)}$. These CF parameters will be further discussed later. It is seen that the the matrix elements of H_{CF} are proportional to the matrix element of the unit tensor operator and therefore become:

$$\begin{aligned} & \langle f^3 W' U' S' L' J' M'_J | H_{CF} | f^3 W U S L J M_J \rangle \\ &= \sum_{kq} A_q^{*(k)} \sum_i \langle r_i^k \rangle (-1)^{J'-M'_J} \begin{pmatrix} J' & k & J \\ -M'_J & q & M_J \end{pmatrix} \delta_{S'S} (-1)^{S+L+J'+k} \\ &\times \left\{ \begin{matrix} L' & L & k \\ J & J' & S \end{matrix} \right\} \sqrt{[J][J']} \sum_{\bar{S}\bar{L}} \langle f^3 W' U' S' L' | \{ f^2(\bar{S}\bar{L}) f W' U' S' L' \rangle \\ &\times \langle f^2(\bar{S}\bar{L}) f W U S L | \{ f^3 W U S L \rangle (-1)^{\bar{L}+f+L'+k} \sqrt{[L][L']} \left\{ \begin{matrix} f & f & k \\ L & L' & \bar{L} \end{matrix} \right\} \\ &\times (-1)^f [f] \begin{pmatrix} f & k & f \\ 0 & 0 & 0 \end{pmatrix} \end{aligned} \quad (3.16)$$

where Eq. (3.9), Eq. (44b) of Racah [4] and Eq. (2.21) have been used.

3.1.4 Configuration interaction (H_{CIL} , H_{CINL}) and other interactions

The fifth and sixth terms of the Hamiltonian are the linear and non-linear configuration interaction terms⁵ (paper IV). These were parameterized during the 1950's and 1960's by Bacher [34], Trees and Jørgensen [35–38], Racah [39], Rajank and Wybourne [40, 41] and Judd [42]. Up until now, only first-order perturbation theory has been used. However, second-order perturbation theory must be called upon to address the problem of CI. The two extra terms appearing in the Hamiltonian (associated with 2-body and 3-body interaction, respectively) are:

$$H_{CIL} = \alpha L^2 + \beta G(G_2) + \gamma G(R_7) \quad (3.17)$$

$$H_{CINL} = \sum_{i=2,3,4,6,7,8} t_i T^i \quad (3.18)$$

Rajnak and Wybourns [40] have derived formulae that account for the following one- and two-electron excitations:

⁵These terms belong to the free-ion Hamiltonian, as opposed to H_{CF} discussed previously.

- i) $l^{N-2}l'^2$ and $l^{N-2}l'l''$
- ii) $l'^{4l'}l^{N+2}$ and $l'^{4l'+1}l''^{4l''+1}l^{N+2}$
- iii) $l'^{4l'+1}l^Nl''$
- iv) $l^{N-1}l'$
- v) $l'^{4l'+1}l^{N+1}$

ii), iii) and v) are core excitations ($4l + 2$ electrons in a filled shell). Rajnak and Wybourne showed that, when including the above excitations (*via* second order perturbation theory), only matrix elements proportional to the following two- and three-particle operators need to be evaluated:

$$\langle f^3W'U'S'L' | \sum_{i<j} (u_i^{(k)} \cdot u_j^{(k)}) | f^3WUSL \rangle \quad (3.19)$$

where $k = 1, 2, \dots, 6$.

$$\langle f^3W'U'S'L' | \sum_{h \neq i \neq j} (\{u_h^{(k)} u_i^{(k')}\}^{(k')} u_j^{(k')})^{(0)} | f^3WUSL \rangle \quad (3.20)$$

Note: that the integrals are evaluated within the $4f$ space. The CI effects proportional to Eq. (3.19) are referred to as the linear configuration interactions, since this effects can be added linearly within the theory; CI effects proportional to Eq. (3.20) are referred to as the non-linear configuration interactions. The matrix elements of Eq. (3.19) with k even are proportional to the Slater integrals and need therefore not be treated further, since the effect is absorbed in the fitting procedure. Matters simplify considerably for k -odd situation when using Eq. (24) of Racah [5], Eq. (19) and Eq. (27) of Racah [6], and the result of Appendix D. From Eq. (D.10) - Eq. (D.12), it is clear that the linear CI effects for k -odd are proportional to the Casimir operators for the groups R_7 , G_2 and R_3 . The radial parameters α , β and γ of Eq. (3.17) are therefore the only additional parameters needed to take account of linear CI effects. The eigenvalues of the different Casimir operators are given by Eq. (D.15) - Eq. (D.17).

The parametrization of the non-linear CI effects Eq. (3.18) has been given by Judd [42]. Judd introduced the t_i operators (using a slightly different notation) as:

$$t(WU) = \sum_{kk'k''} \langle kk'k'' | WU \rangle U(kk'k'') \quad (3.21)$$

where $U(kk'k'')$ is a triple-tensor given by:

$$U(kk'k'') = \sum_{q,q',q''} ([k][k'][k''])^{1/2} \begin{pmatrix} k & k' & k'' \\ q & q' & q'' \end{pmatrix} \sum_{h \neq i \neq j} (\{u_h^{(k)} u_i^{(k')}\}^{(k')} u_j^{(k')})^{(0)} \quad (3.22)$$

[e.g. Eq. (3.20)]. The matrix elements of this operator can be evaluated using the following formulae; see Rajnak [41] and Tables VI, VII of Judd [42]:

$$\langle \psi | t(WU) | \psi' \rangle = \sum_{kk'k''} \langle kk'k'' | WU \rangle ([k][k'][k''])^{1/2}$$

$$\begin{aligned}
& \times \sum_{q,q',q''} \begin{pmatrix} k & k' & k'' \\ q & q' & q'' \end{pmatrix} \langle \psi | \sum_{h,i,j} (\{u_h^{(k)} u_i^{(k'')} \}^{(k')} u_j^{(k')})^{(0)} | \psi' \rangle \\
& - \left\{ \begin{matrix} k & k' & k'' \\ f & f & f \end{matrix} \right\} \left[\langle \psi | (u^{(k)})^2 | \psi' \rangle + \langle \psi | (u^{(k')})^2 | \psi' \rangle \right. \\
& \left. + \langle \psi | (u^{(k'')})^2 | \psi' \rangle - \delta(\psi, \psi') 2N/[f] \right] \tag{3.23}
\end{aligned}$$

where the matrix element of the triple tensor operator is given by:

$$\begin{aligned}
& \langle \psi | \sum_{h,i,j} (\{u_h^{(k)} u_i^{(k'')} \}^{(k')} u_j^{(k')})^{(0)} | \psi' \rangle \\
& = \sum_{\bar{\psi}\bar{\psi}'} \left\{ \begin{matrix} k & k' & k'' \\ \bar{L}' & \bar{L} & L \end{matrix} \right\} \langle \psi || u^{(k)} || \bar{\psi} \rangle \langle \bar{\psi} || u^{(k'')} || \bar{\psi}' \rangle \\
& \times \langle \bar{\psi}' || u^{(k')} || \psi' \rangle / [L] \tag{3.24}
\end{aligned}$$

The matrix elements of the double tensor operators appearing in Eq. (3.23) are essentially the same as in Eq. (3.6), and the matrix elements of the single tensor operators appearing in Eq. (3.24) are essentially the same as in Eq. (3.16).

There are several more Hamiltonians to be considered in a more elaborate calculation, e.g. the spin-spin (H_{ss}), spin-other-orbit (H_{soo}), and CI effects on the spin-orbit (H_{ci}) Hamiltonian. These operators will give rise to the additional parameters M^k (Marvin integrals) and P^k ; see Judd, Crosswhite and Crosswhite [43,44] for more detail. Rajnak and Wybourne [45] investigated the effects of CI on crystal field effects and concluded that these should be small for the rare earths. None of these last four effects has been treated in this thesis.

Other papers not referred to so far but nevertheless important for the energy matrix are given in [46]; or those important for the parameter fitting procedure in [47].

3.2 The radial wave functions

So far, the theory has treated only the angular part of Eq. (2.1); The radial part remains to be accounted for. All parameters in the preceding sections are different types of integrals over the radial wave functions. If these could be computed correctly, we would have achieved a “first-principles” treatment. We, as others before us, have found (paper **III**) that the radial wave functions calculated with standard Hartree-Fock codes⁶ give values which are too small (large Slater integrals). The values of integrals of the type $\langle r^k \rangle$ are acceptable (at least for $k \leq 4$) since these are not especially sensitive to the shape of the wave function. However, in attempting to calculate (for example) the Slater integrals (F^k), the results are certainly not satisfactory.

⁶We have used different approaches using a standard Desclaux code, the well known code of Cowan and the Froese-Fischer code (Parpia *et al.* [48]).

3.3 The crystal field parameters ($A_q^{(k)}$)

The treatment of the crystal field and how it interacts with the rare-earth ions should be seen as the most important part of this thesis (paper **II**). If the CF model used is selected carefully, the potential range of application of the calculation method described can be very large. It was shown in Section 3.1.3 that rare-earth ion interactions with the surroundings can be described through the crystal field parameters $A_q^{(k)}$, provided $1/(r_i - r_j)$ can be expanded in Legendre polynomials. If there is no radial overlap, i.e. Laplace's equation is satisfied between the ions, the charge density that the rare-earth ions experience can be expressed in an electrostatic multipole expansion. This approximation is not too crude for ionic compounds but other techniques must be used when considering more covalent materials; e.g. the standard linear combination of atomic orbitals (LCAO) approach. The compounds studied herein can be considered as ionic, for which the electrostatic model should therefore be fairly adequate. The electrostatic model is often criticised for its lack of sophistication. However, as will be shown later, more severe problems exist than those associated with the amplitude of the static correction; more sophisticated models may be found in [49–54]. The $A_q^{(k)}$ parameters are defined by the integral:

$$A_q^{(k)} = - \int dr' \frac{\rho(r') C_q^{(k)}(\hat{r}')}{r'^{t+1}} \quad (3.25)$$

In the electrostatic model, $\rho(r')$ can be expanded as a sum of 2^n -poles ($n=0,1,2,\dots$). $A_q^{(k)}$ is thus given approximately by Burns [55] (paper **II**, **III**):

$$A_q^k = \sum_j \left(M_j^{(0)} r_j^{t-k-1} + D_j^{(1)} (k+1) r_j^{t-k-2} + \frac{1}{2} Q_j^{(2)} (k+1)(k+2) r_j^{t-k-3} + \dots \right) C_q^{(k)}(\hat{r}_j) \quad (3.26)$$

where $M^{(0)}$, $D^{(1)}$ and $Q^{(2)}$ are the components of the mono-, di- and quadrupole moments, respectively. Following Faucher and Garcia [56], these are given by:

$$D_{\hat{r}} = \hat{r}^s \bar{D}_s \quad (3.27)$$

$$Q_{\hat{r}} = \hat{r}^s \hat{r}^t \bar{Q}_{st} \quad (3.28)$$

\hat{r} is the unit vector directed from the rare-earth ion towards the the neighbouring ion; s and t are indices for the vector and tensor components, not to be confused with i or j which label the ions:

$$M_i^{(0)} = q_i \quad (3.29)$$

$$\bar{D}_i^{(1)} = -\alpha_i^{(1)} \sum_{j \neq i} \left\{ \nabla \frac{1}{|\bar{r}_{ij}|} + \bar{D}_j^{(1)} \nabla \nabla \frac{1}{|\bar{r}_{ij}|} + \bar{Q}_j^{(2)} \nabla \nabla \nabla \frac{1}{|\bar{r}_{ij}|} \right\} \quad (3.30)$$

$$\bar{Q}_i^{(2)} = \alpha_i^{(2)} \sum_{j \neq i} \left\{ \nabla \nabla \frac{1}{|\bar{r}_{ij}|} + \bar{D}_j^{(1)} \nabla \nabla \nabla \frac{1}{|\bar{r}_{ij}|} \right\} \quad (3.31)$$

The $A_q^{(k)}$ parameters must be corrected, since the closed shells of the rare-earth ion will not remain unaffected when exposed to the crystal field. This correction is taken into account by a redefinition of the CF parameters: $A_q^{(k)} \rightarrow (1-\sigma_k) A_q^{(k)}$, where σ_k are the shielding parameters (paper **III**).

The summation (3.26) is performed until convergence of the $A_q^{(k)}$ parameters is achieved. The dipole and quadrupole polarizabilities used are obtained from the *ab initio* calculations

of Schmidt *et al.* [57] and Mahan [58] (paper **III**). All dipole moments are calculated self consistently, i.e. electrostatic equilibrium of charges and induced dipoles at each ion-site is assured. This is accomplished by rewriting (3.30) and solving the linear system of equations:

$$\bar{D}^{(1)} = \left(\bar{\mathbb{I}} + \alpha^{(1)} \bar{\bar{T}} \right)^{-1} \alpha^{(1)} \bar{E}' \quad (3.32)$$

$\alpha^{(1)} \bar{E}'_i$ is given by

$$-\alpha_i^{(1)} \sum_{j \neq i} \left\{ \nabla \frac{1}{|\bar{r}_{ij}|} + \bar{\bar{Q}}_j^{(2)} \nabla \nabla \nabla \frac{1}{|\bar{r}_{ij}|} \right\}$$

and $\bar{\bar{T}}_{ij}$ is given by:

$$\bar{\bar{T}}_{ij} = -\nabla \nabla \frac{1}{|\bar{r}_{ij}|} = \frac{1}{r_{ij}^3} \left(\bar{\mathbb{I}} - 3 \frac{\bar{r}_{ij} \bar{r}_{ij}}{r_{ij}^2} \right) \quad (3.33)$$

The Ewald method (paper **VII**) would, of course, be preferable to direct summation. This technique for performing infinite lattice sums will be implemented in future work.

3.4 Diagonalization and numerical detail

There is no doubt that some numerical difficulties will be encountered when performing this type of simulation. For the cases of Nd^{3+} or Er^{3+} , the energy matrix have $364^2 = 132496$ matrix elements; expression for each of these has been given above⁷. Since almost all Physics is hermitian, only half of the matrix has to be evaluated using the preceding sections. The other half is simply the complex conjugate of the corresponding elements mirrored in the diagonal. The LAPACK routine *ZHEEV* has been used for diagonalizing, and the LAPACK routine *DEGSV* has been used to solve the system of linear equations encountered in Section 3.3. The calculations were performed primarily on a number of Pentium PRO 200 MHz processors. A typical simulation (including MD and the calculation of oscillator strengths) of a polarized absorption spectrum with contributions from 200 different environments would need approximately 2 weeks on 3 processors of this type.

The biggest numerical challenge, however, was the calculation of the shielding parameters, and the dipole and quadrupole polarizabilities. Details are presented in paper **III** of this thesis.

Figure 3.1 shows the free-ion energy matrix for Nd^{3+} after diagonalization. It is seen that the lower energy states have a low level of mixing, so the problem with labelling is not so severe. The situation is more serious for the higher energy states, where the eigenvectors are a mixture of many states.

⁷For the rare earths with more complicated $4f$ structure, the number of matrix elements is even larger: $4f^{4,10} \rightarrow 1002001$, $4f^{5,9} \rightarrow 4008004$, $4f^{6,8} \rightarrow 9018009$, $4f^7 \rightarrow 11778624$.

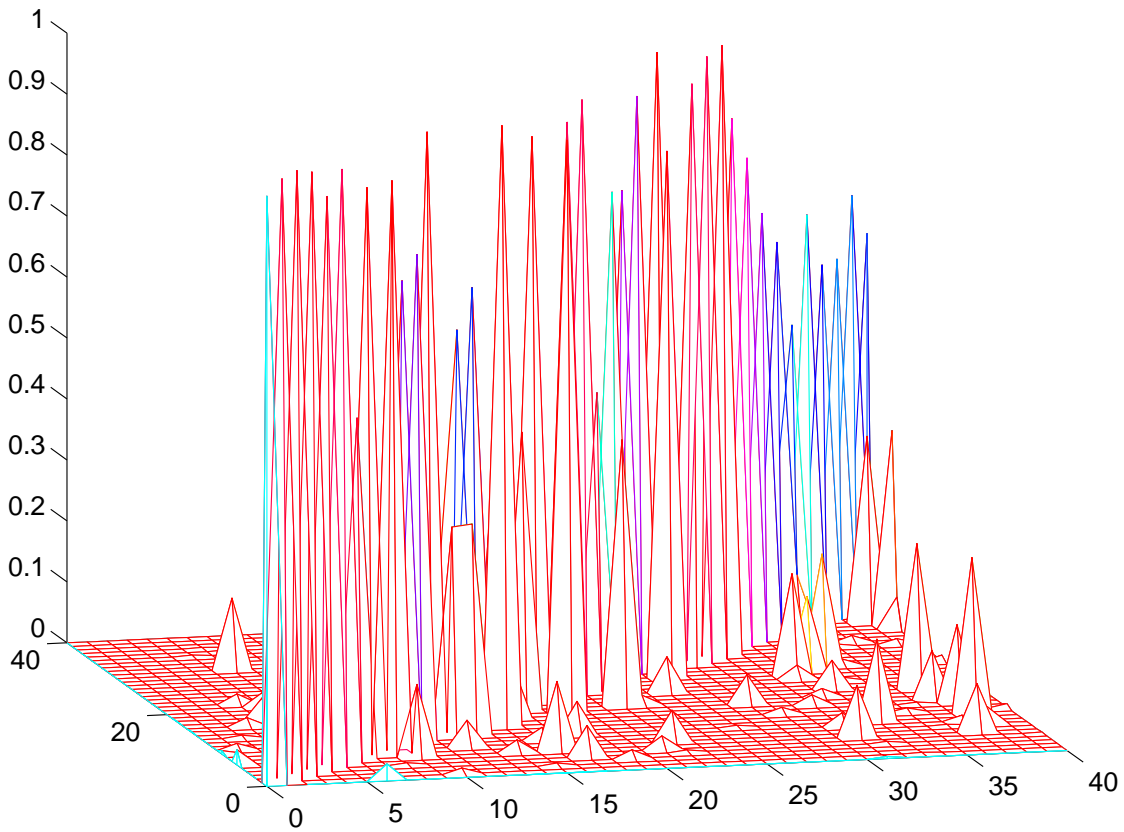


Figure 3.1: The free-ion eigenvectors for Nd^{3+} . The x and y axis shown the term number (41 for Nd^{3+}).

Chapter 4

The oscillator strengths; absorption/emission spectra

4.1 Introduction

In 1962, Judd [8] and Ofelt [9] published their classic papers which outlined the theory for electric dipole transitions between J -manifolds in the $4f$ shell of rare-earth ions. This theory has been quite successful in predicting oscillator strengths. In these calculations, only the electric dipole mechanism and inhomogeneous dielectric mechanism have been considered; the latter is sometimes small. The contributions from electric quadrupole and magnetic dipole transitions have not been included, since these are usually one order of magnitude smaller. In the first footnote of this thesis it was shown that the position and parity operators do not commute ($[r, \pi] \neq 0$, $\{r, \pi\} = 0$). This implies that electric dipole transitions are parity forbidden within the $4f$ shell. This is easily shown:

$$\langle i | r | f \rangle = \langle i | \pi^\dagger \pi r \pi^\dagger \pi | f \rangle = \epsilon_i \epsilon_f (- \langle i | r | f \rangle) \quad (4.1)$$

which can only be true if ϵ_i and ϵ_f have opposite signs, i.e. $\langle i |$ and $| f \rangle$ have opposite parities. That transitions take place between eigenstates of opposite parity is known as the *Laporte's rule*. As a consequence, non-zero matrix elements for the dipole operator can only be accomplished if the eigenstates have a small addition of opposite parity. This is indeed the case and is a result of the crystal field experienced by the rare-earth ion.

4.2 Judd-Ofelt theory and refinements

Judd and Ofelt showed that the matrix element of the dipole operator

$$D_q^{(1)} = \sum_j r_j C_q^{(1)}(\hat{r}_j) \quad (4.2)$$

which includes the addition of opposite parity states through first-order perturbation theory [using the odd part of the crystal field operator ($A_q^{(k)}$ with k odd)], can be expressed as a matrix element involving only $4f$ states. The closure approximations used are considered to be accurate.

The expression they obtained is:

$$P = \sum_{\lambda=2,4,6} T_{\lambda\nu} |\langle f^3 W' U' S' L' || U^{(\lambda)} || f^3 W U S L \rangle|^2 \quad (4.3)$$

where

$$T_\lambda = \chi \frac{8\pi^2 m[\lambda]}{3h[J]} \sum_{kq} \frac{\Xi^2(k, \lambda)}{[k]} |A_q^{(k)}|^2 \quad (4.4)$$

The factors 3 and $[J]$ in the denominator come from the fact that the polarization is averaged out, and that all Stark levels are assumed degenerate.

$$\begin{aligned} \Xi(k, \lambda) &= 2 \sum_{n'l'} [l][l'] (-1)^{l+l'} \begin{Bmatrix} 1 & \lambda & k \\ l & l' & l \end{Bmatrix} \begin{pmatrix} l & 1 & l' \\ 0 & 0 & 0 \end{pmatrix} \begin{pmatrix} l' & k & l \\ 0 & 0 & 0 \end{pmatrix} \\ &\times \frac{\langle nl | r | n'l' \rangle \langle nl | r^k | n'l' \rangle}{\Delta E(n'l')} \end{aligned} \quad (4.5)$$

Note that the radial wave functions and energies must be obtained from elsewhere, usually a Hartree-Fock calculation; χ is the Lorentz local field correction, given by $\chi = (n^2 + 2)^2 / (9n)$, once the refractive index (n) is known; m is the electron mass, and ν the transition frequency.

As pointed out above, Eq. (4.3) gives only the unpolarized oscillator strength between the J -manifolds. If the polarized oscillator strengths between individual Stark levels are to be calculated, this equation needs modification. Such a modification has been given in [59–63] (papers **I** and **II**). The polarization was averaged out in [59, 61]. Following Edvardsson [63], the formula becomes:

$$P_q = \frac{1}{2} \chi \frac{8\pi^2 m\nu}{h} |\langle i | D_q^{(1)} | f \rangle|^2 \frac{e^{-E_i/k_B T}}{\sum e^{-E_i/k_B T}} \quad (4.6)$$

where

$$\begin{aligned} &\langle i | D_q^{(1)} | f \rangle \\ &= \sum_{\lambda k q' i f} [\lambda] (-1)^{q'+q} A_{q'}^{(k)} \begin{pmatrix} 1 & \lambda & k \\ q & -q' - q & q' \end{pmatrix} a_i^* a_f (-1)^{J_i - M_i} \\ &\times \begin{pmatrix} J_i & \lambda & J_f \\ -M_i & q' + q & M_f \end{pmatrix} \langle f^3 W' U' S' L' J' \| U^{(\lambda)} \| f^3 W U S L J \rangle \Xi(k, \lambda) \end{aligned} \quad (4.7)$$

The factor 1/2 in Eq. (4.6) is due to the *Kramer degeneracy*. The coefficients a_i and a_f are the components of the eigenvectors (paper **I**). Note also that Eq. (4.6) is only valid for absorption, since the ground state levels are assumed to be Boltzmann populated. A corresponding equation for emission can be obtained, see below; $\Xi(k, \lambda)$ is given by Eq. (4.5), and the reduced matrix element of the unit tensor operator, which is essentially the same as Eq. (3.16), is given by:

$$\begin{aligned} &\langle f^3 W' U' S' L' J' \| U^{(\lambda)} \| f^3 W U S L J \rangle \\ &= (-1)^{S+L'+\lambda-J} \sqrt{[J][J']} \begin{Bmatrix} L & L' & \lambda \\ J' & J & S \end{Bmatrix} \\ &\times \sum_{\bar{S}\bar{L}} \langle f^3 W' U' S' L' \{ f^2(\bar{S}\bar{L}) f W' U' S' L' \} \rangle \langle f^2(\bar{S}\bar{L}) f W U S L \{ f^3 W U S L \} \rangle \\ &\times \sqrt{[L][L']} (-1)^{\bar{L}+l+L+\lambda} \begin{Bmatrix} l & l & \lambda \\ L' & L & \bar{L} \end{Bmatrix} \end{aligned} \quad (4.8)$$

$\langle i |$ and $| f \rangle$ are the initial and final eigenstates for the rare-earth ion.

4.2.1 The inhomogeneous dielectric mechanism

In addition to electric dipole transitions, the *inhomogeneous dielectric mechanism* (IDM) of Jørgensen and Judd [64,65] has also been considered (papers **IV** and **V**). The IDM is based on the assumption that the radiation field induces oscillating dipole moments in the ligands. The CF seen by the rare-earth ion will therefore have a stronger quadrupole component than would be expected. This will, in turn, allow even-order electric multipole transitions within the $4f$ shell. In addition to Eq. (4.7), the following matrix element, given by [62, 66, 67], must be evaluated:¹

$$\begin{aligned}
& \langle i | W_q^{IDM} | f \rangle \\
&= \sum_{\lambda k q' i f} \delta_{\lambda+1, k} \sqrt{[k](\lambda+1)[\lambda](1-\sigma_\lambda)} A_{q'}^{(k)IDM} (-1)^l [l] \begin{pmatrix} l & \lambda & l \\ 0 & 0 & 0 \end{pmatrix} (-1)^{q'+q} \quad (4.9) \\
&\times \begin{pmatrix} 1 & \lambda & \lambda+1 \\ q & -q'-q & q' \end{pmatrix} a_i^* a_f (-1)^{J_i-M_i} \begin{pmatrix} J_i & \lambda & J_f \\ -M_i & q'+q & M_f \end{pmatrix} \\
&\times \langle f^3 W' U' S' L' J' \| U^{(\lambda)} \| f^3 W U S L J \rangle \quad (4.10)
\end{aligned}$$

where $A_{q'}^{(k)IDM}$ is given by:

$$A_{q'}^{(k)IDM} = \sum_j \alpha_j r_j^{l-k-1} C_{q'}^{(k)}(\hat{r}_j) \quad (4.11)$$

The reduced matrix element of the unit tensor operator is given by Eq. (4.8). No extraordinarily strong contributions from the IDM have been seen in this work. This might indicate that the IDM is not responsible for the hypersensitivity observed for certain transitions. Molecular dynamics (or any equivalent method) should be used instead to simulate the various environments of the system directly; see Edvardsson [63, 68] for a more rigorous discussion. In this way, no new mechanism need be introduced to explain hypersensitivity. This aspect will be returned to later.

4.2.2 Other effects

Electric quadrupole and magnetic dipole transitions have not been considered since these are believed to be very weak in most cases. A rigorous calculation should, of course, include such effects.

If the compound under investigation is optically isotropic, oscillator strengths can be averaged over q and calculated according to:

$$P = \frac{1}{3} \sum_q P_q \quad (4.12)$$

In standard Judd-Ofelt theory, Ω_λ are the parameters of interest; Ω_λ are given by:

$$\Omega_\lambda = [\lambda] \sum_{kq'} \frac{|A_{q'}^{(k)} \Xi(k, \lambda)|^2}{[k]} \quad (4.13)$$

¹This matrix element is rather different from the original Judd/Ofelt calculation, since no opposite-parity states have to be mixed-in here.

4.3 Absorption/emission spectra

As noted above, it is not difficult to pass from absorption to emission once Eq. (4.6) is known. The major difference between absorption and emission is the population of the states. A standard Boltzmann population is assumed for absorption. This will not be true, however, for the excited states, where the population must be calculated. Luckily, Eq. (4.6) compares well with experiment [if the energy matrix is calculated according to Chapter (3)]. This means that the population of the excited states can be obtained from Eq. (4.6), after renormalization. The scheme for calculating emission transitions becomes:

- 1) Calculate and diagonalize the energy matrix.
- 2) Calculate the polarized absorption oscillator strengths.
- 3) Populate the excited states according to the results of 2).
- 4) Use Eq. (4.6) with the Boltzmann factor replaced by 3) to compute the polarized emission oscillator strengths.

4.4 Results

The calculation of σ - and π -polarized absorption spectra is demonstrated for $\text{Nd}^{3+}:\text{LiYF}_4$ (papers **IV** and **VI**), $\text{Nd}^{3+}:\text{YAG}$ (papers **II** and **IV**), Nd_2O_3 (paper **VI**) and $\text{Er}^{3+}:\text{Y}_2\text{O}_3$ (paper **V**). With the exception of Nd_2O_3 , these calculated spectra are compared with experiment. CI effects and electric-dipole and inhomogeneous dielectric mechanisms are included for $\text{Nd}^{3+}:\text{LiYF}_4$, $\text{Nd}^{3+}:\text{YAG}$ and $\text{Er}^{3+}:\text{Y}_2\text{O}_3$. No CI effects have been considered for Nd_2O_3 , nor has the inhomogeneous dielectric mechanism been taken into account.

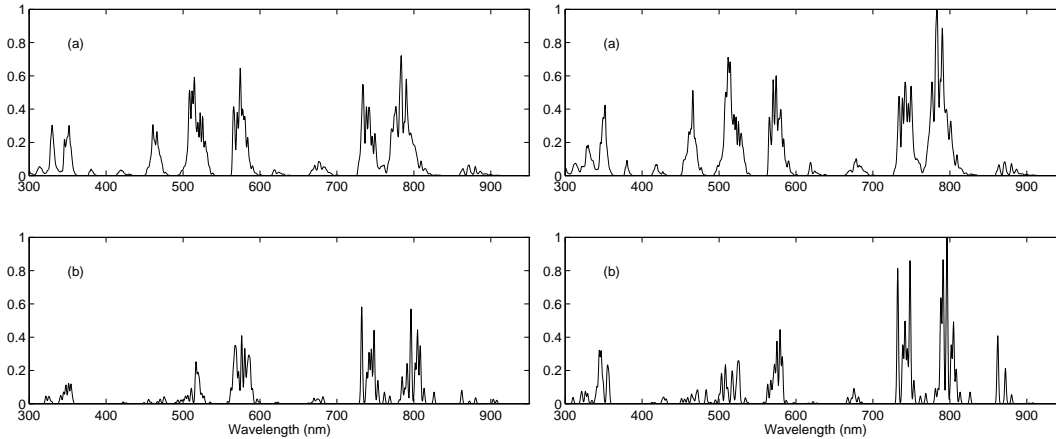


Figure 4.1: (a) The calculated absorption intensities for all transitions ${}^4\text{I}_{9/2} \rightarrow {}^4\text{F}_{3/2} - {}^2\text{D}_{5/2}$ at 300 K for σ -polarized $\text{Nd}^{3+}:\text{LiYF}_4$. (b) The experimental absorption spectrum of σ -polarized $\text{Nd}^{3+}:\text{LiYF}_4$ (1.5 wt.% Nd^{3+}) at 300 K. The intensities are in arbitrary units.

Figure 4.2: (a) The calculated absorption intensities for all transitions ${}^4\text{I}_{9/2} \rightarrow {}^4\text{F}_{3/2} - {}^2\text{D}_{5/2}$ at 300 K for π -polarized $\text{Nd}^{3+}:\text{LiYF}_4$. (b) The experimental absorption spectrum of π -polarized $\text{Nd}^{3+}:\text{LiYF}_4$.

Figures 4.1 and 4.2 show the results for $\text{Nd}^{3+}:\text{LiYF}_4$. The experimental spectrum is taken from Ryan and Beach [69]; the paper also contains the different CI parameters used. These are shown in Table II of paper IV. The agreement with experiment is generally good.

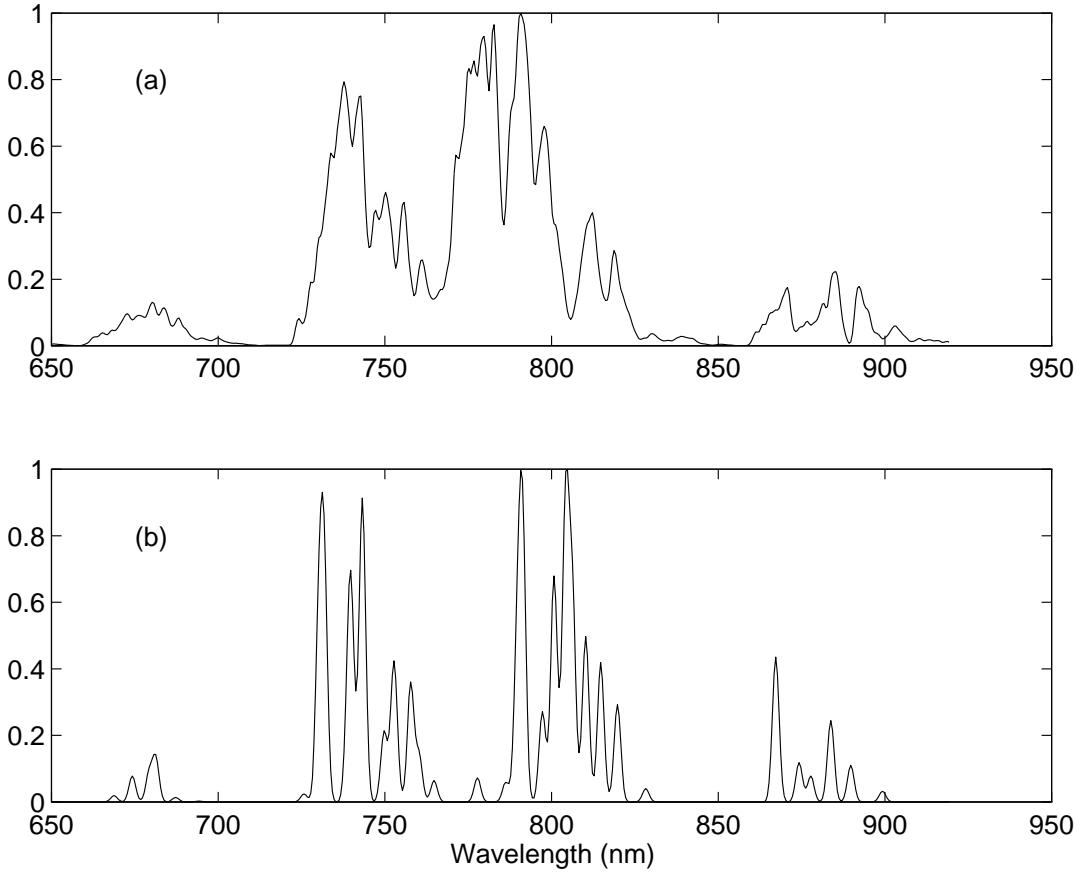


Figure 4.3: (a) The calculated absorption intensities for all transitions ${}^4\text{I}_{9/2} \rightarrow {}^4\text{F}_{3/2-2}\text{D}_{5/2}$ at 300 K for $\text{Nd}^{3+}:\text{YAG}$. (b) The experimental absorption spectrum of $\text{Nd}^{3+}:\text{YAG}$ (1.0 wt.% Nd) at 300 K. The intensities are in arbitrary units.

Figure 4.3 shows good agreement with experiment (Kramer and Boyd [70]) for $\text{Nd}^{3+}:\text{YAG}$. The peak widths in the calculated spectrum are slightly too large, which suggests that the ions are “too mobile” in the MD simulation. This aspect will be discussed in the next chapter. Since $\text{Nd}^{3+}:\text{YAG}$ is optically isotropic, the oscillator strengths have been calculated as the average of P_q (summation over $q=-1,0,1$); see Eq. (4.12).

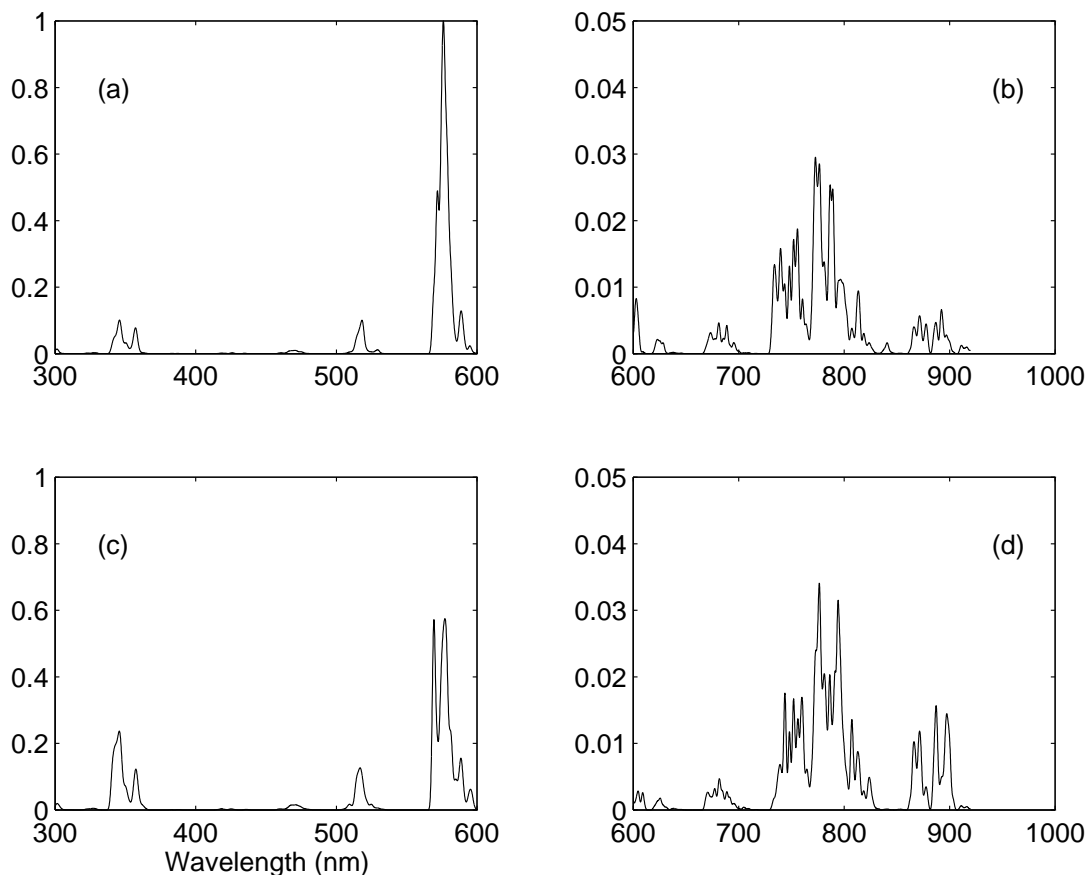


Figure 4.4: The calculated absorption intensities for all transitions from ${}^4I_{9/2}$ to ${}^4F_{3/2-2}D_{5/2}$ at 300 K for Nd_2O_3 . (a) and (b) show the π -polarized contribution to the spectrum. (c) and (d) show the σ -polarized contribution. Note the difference in scale between (a), (b) and (c), (d).

The theoretical oscillator strengths for Nd_2O_3 calculated for all the ${}^4I_{9/2} \rightarrow {}^4F_{3/2-2}D_{5/2}$ transitions at 300 K are plotted in Figure 4.4. It is interesting to note the large oscillator strengths around 570 nm. These are the hypersensitive transitions, which are partly explained by the large $\langle {}^4I_{9/2} \| U^{(2)} \| {}^4G_{5/2} \rangle$ value [64, 65], and by the sensitivity of $A_q^{(1)}$ and $A_q^{(3)}$ to changes in environment (Edvardsson [63, 68]). Note that no inhomogeneous dielectric mechanism have been considered in this calculation. No experimental spectrum is available.

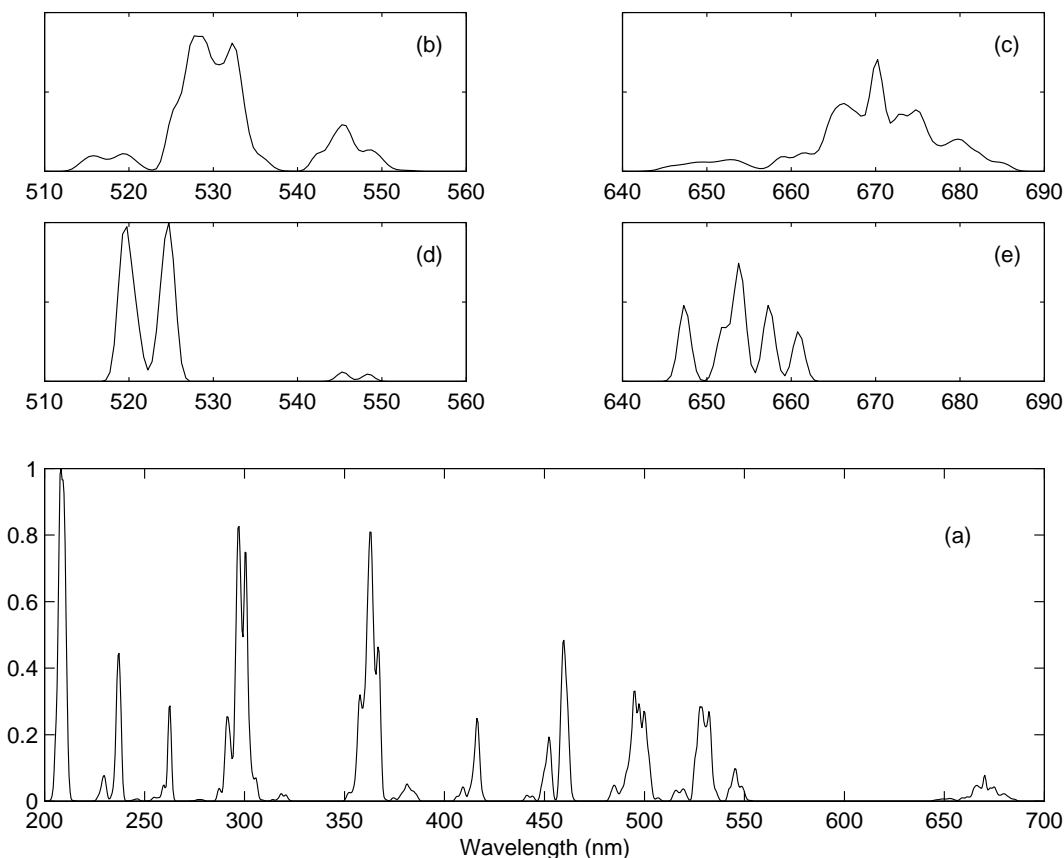


Figure 4.5: The calculated absorption spectrum for $\text{Er}^{3+}:\text{Y}_2\text{O}_3$ in arbitrary units (a). The calculated spectra (a, b and c) are plotted with the C_2 and C_{3i} contributions weighted; the experimental spectra are plotted in (d) and (e).

The calculated absorption spectrum for $\text{Er}^{3+}:\text{Y}_2\text{O}_3$ are shown in Figure 4.5. Since $\text{Er}^{3+}:\text{Y}_2\text{O}_3$ is cubic, Eq. (4.12) can be used to calculate the oscillator strengths. The only experimental absorption spectrum available (Morrison *et al.* [60]) is plotted in (d) and (e). Plots (b) and (c) are the corresponding calculated transitions with the C_2 and C_{3i} contributions weighted. The qualitative agreement between experiment and theory is again clear as regards the overall shape of the transition manifolds; we see, however, that the multiplets are shifted slightly to lower energies. This is a consequence of uncertainties in the free-ion parameters. The case of $\text{Er}^{3+}:\text{Y}_2\text{O}_3$ will be returned to in Chapter 6 because of its two different erbium sites. It will be seen that, for some transitions, the contribution from ions in the C_{3i} -site cannot be ignored, despite the fact that the site is a crystallographic inversion centre.

It must be remembered that, prior to our refinement of the Judd-Ofelt theory, in most intensity calculations the Stark level transitions were treated as degenerate. In Figure 4.6 (c) Judd-Ofelt intensities have been assigned to each Stark transition for $\text{Nd}^{3+}:\text{YAG}$. The differences are clear.

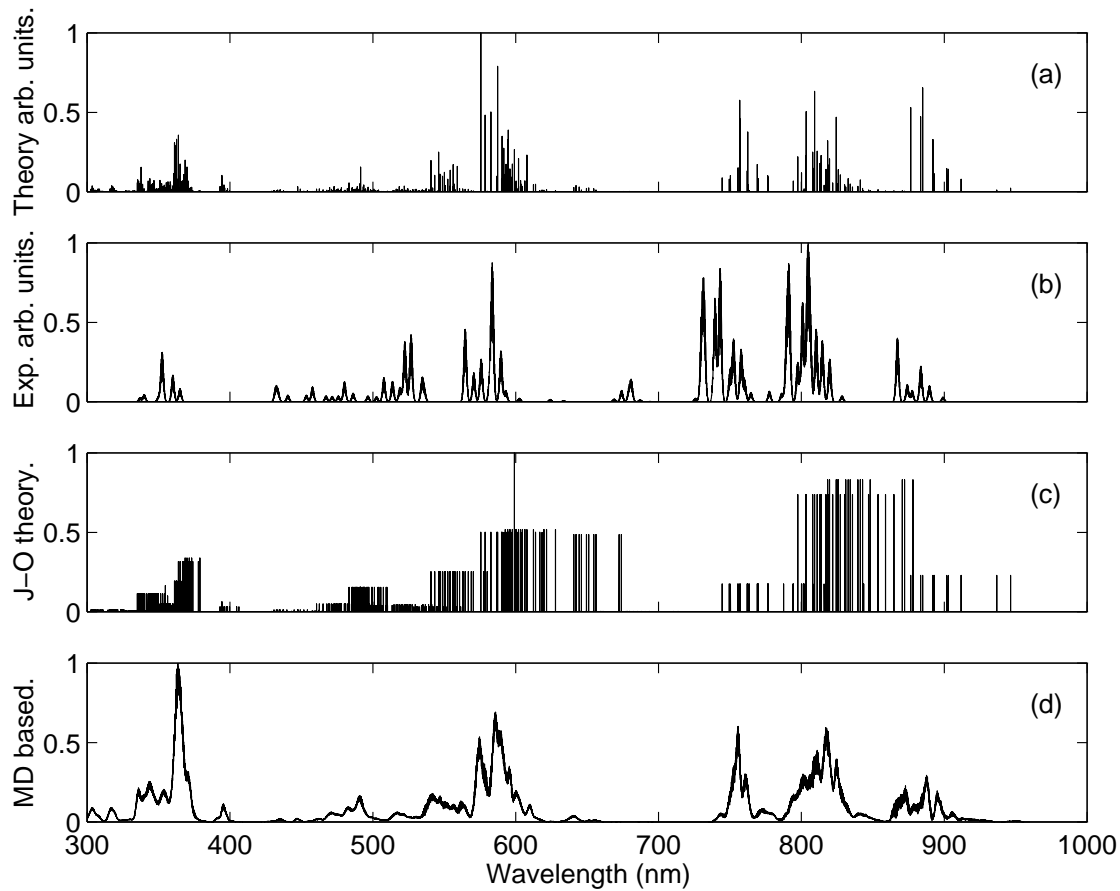


Figure 4.6: (a) The calculated absorption intensities for all transitions from ${}^4I_{9/2}$ to ${}^4F_{3/2}$ - ${}^2D_{5/2}$ at 300 K. (b) The experimental absorption spectrum for 1 wt% Nd:YAG at 300 K. (c) The calculated absorption spectrum, when Judd-Ofelt intensities have been assigned to each Stark transition. (d) The absorption spectrum summed over 100 configurations obtained from an MD simulation at 300 K.

Figure 4.6(a) shows the first calculation for $\text{Nd}^{3+}:\text{YAG}$. No CI effects and no inhomogeneous mechanism were considered; only crystallographic ion-sites were used. (b) is the experimental spectrum, and (d) the result after the MD based treatment. Figures 4.6(c) and 4.3 should be compared to gain an impression of the importance of refinements and the MD treatment.

The MD treatment allows inhomogeneous line broadening to be seen in all spectra. See, for example, Figure 4.6(d).

Chapter 5

Molecular dynamics simulation

5.1 Introduction

The molecular dynamics (MD) simulation technique has been shown to be an important tool in calculating polarized absorption/emission oscillator strengths and the corresponding spectra (papers **I**, **II**, **IV** and **V**). Instead of merely using the experimentally determined crystal structure in the crystal field calculations, MD simulation generates an ensemble of physically realistic environments for the rare-earth ions. Details of the MD technique used can be found in [63, 71, 72]; an alternative approach is presented in [73, 74]. The crystal field parameters have shown to fluctuate greatly as a consequence of the many different rare-earth environments. These fluctuations would appear to be somewhat too large, since the calculated spectra are broader than the corresponding experimental spectra. This can probably be taken as an indication that the MD potentials used should be reexamined (which is not surprising since the potential parameters are only fitted to reproduce the crystal structure; moreover only a simple pair-potential has been used). The incorporation of the Debye-Waller factors into the fitting procedure and the use of a many-body potential would probably improve the simulation, as regards the band-widths. The fluctuations in the CF parameters implies that the energy matrix must be recalculated for each MD generated environment in order to get the new Stark energies and transition probabilities.

The MD simulation has made it possible to calculate transition probabilities for rare-earth ions in sites with inversion symmetry, e.g. C_{3i} in $\text{Er}^{3+}:\text{Y}_2\text{O}_3$ (paper **V**), and to address the case of hypersensitive transitions (see Edvardsson [63, 68]). Granted the availability of more reliable MD potentials, both line-shape as well as the analysis of a local structure for amorphous systems can be accessed by the method.

5.2 The theory

A molecular dynamics approach involves the solution of the $3N$ coupled Newton's equations of motion for an N particle system. The equation for the i -th particle is:

$$m_i \ddot{\vec{r}}_i = \vec{F}_i = -\vec{\nabla} V_i \quad (i = 1, \dots, N) \quad (5.1)$$

where V_i is the ion-ion potential in Born-Mayer-Huggins form:

$$V_i = \sum_{i \neq j}^N q_i q_j / r_{ij} + A_{ij} \exp(-r_{ij} / \rho_{ij}) - C_{ij} / r_{ij}^6 \quad (5.2)$$

The three terms in Eq. (5.2) are: a long-range Coulombic term, a short-range repulsive term, and a weak van der Waals term. The potential parameters A_{ij} , ρ_{ij} and C_{ij} are fitted to reproduce a known crystal structure.

The MD system is assumed to be isolated, i.e. the microcanonical ensemble has been assumed with conservation of the total energy E , the volume V , and the number of particles N . A more advanced ensemble must be used in a more rigorous MD treatment. The simulation is initialized by assigning the velocities according to a Maxwell-Boltzmann distribution: $p_r = (1/Z) \exp(-\beta E_r)$, where $Z = \sum_r \exp(-\beta E_r)$ and $\beta = 1/(k_B T)$; p_r is the probability for a system in state r with temperature T and energy E_r . This assignment is followed by an equilibration phase of for several thousand time-steps, $\Delta T = 3$ fs. The system is said to be equilibrated when the target temperature is reached.

Periodic boundary conditions are used and the Ewald summation technique (Ewald [75]) is exploited to take accurate account of the long-range coulomb interaction. The technique is outlined briefly in paper VII.

5.3 Results

The solution to Newton's equations of motion involves the positions, velocities and accelerations for each of the particles in the simulation box at each time step.

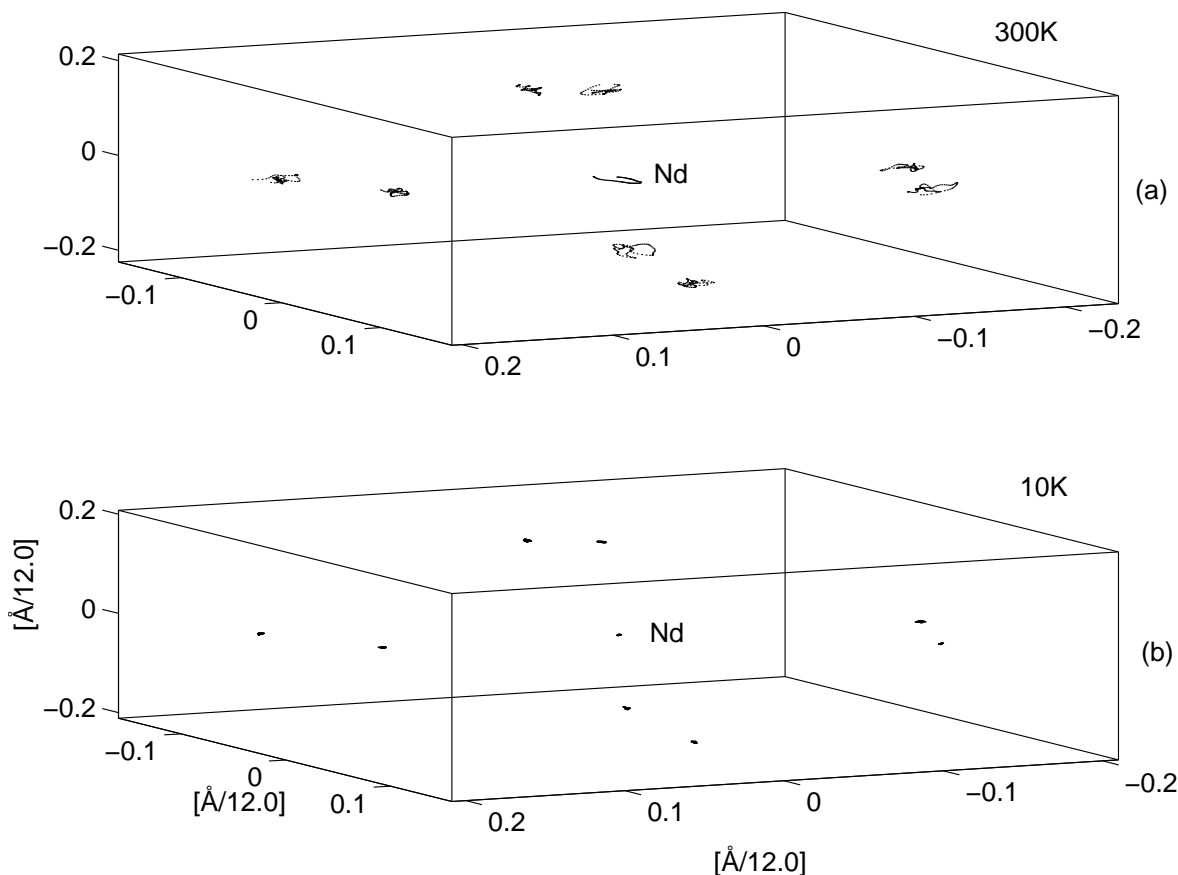


Figure 5.1: The trajectories of a Nd³⁺-ion and its nearest-neighbours at 300 K (a) and 10 K (b) in Nd³⁺:YAG. The figure includes 100 snapshots.

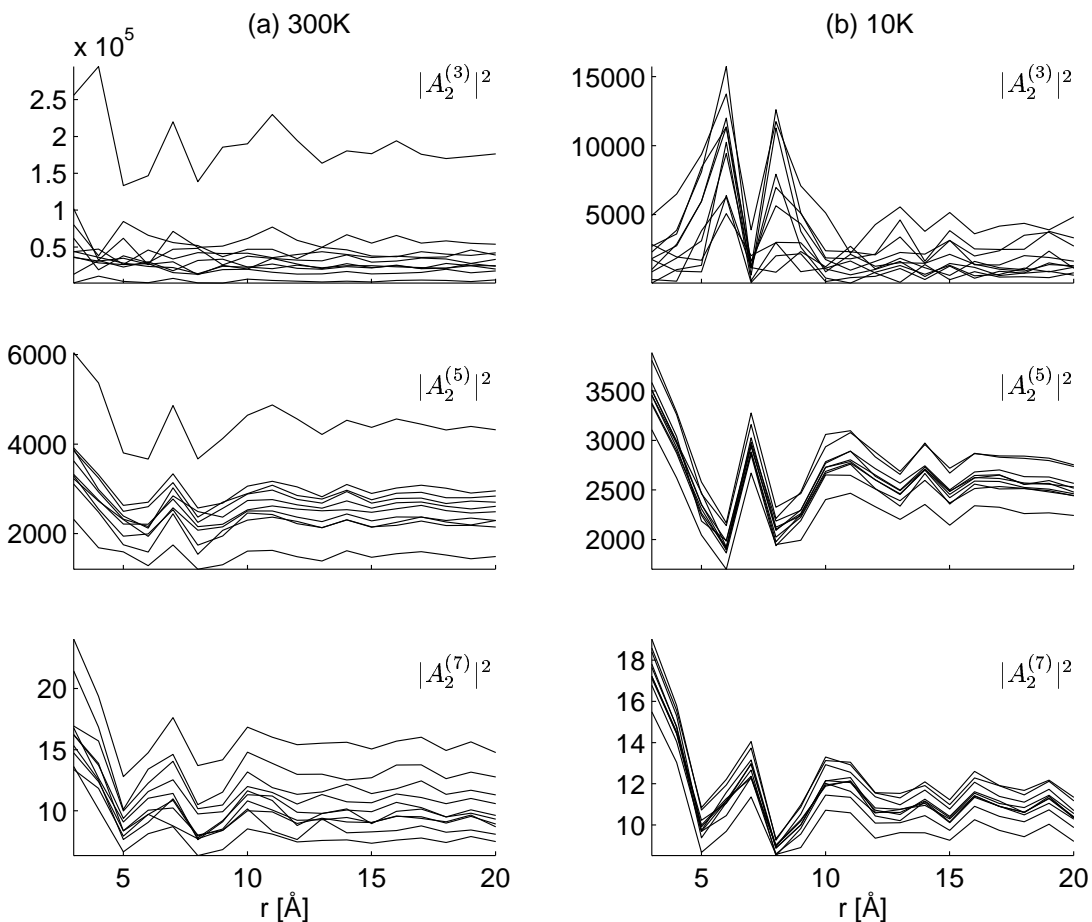


Figure 5.2: Convergence plots for $|A_q^{(k)}|^2$ [$\text{cm}^{-(k+1)}$] as a function of the radius of the summation sphere around the Nd^{3+} -ion for ten typical Nd^{3+} -ion environments at (a) 300K and (b) 10K.

Taking an example: the trajectories for a Nd^{3+} and its eight nearest neighbours in $\text{Nd}^{3+}:\text{YAG}$ have been plotted in Figure 5.1. The figure shows 100 snapshots at $T=300\text{K}$ and $T=10\text{K}$. Figure 5.2 shows the convergence of $|A_q^{(k)}|^2$ as a function of r , the radius of the summation sphere, at 300K and 10K for the environments of ten different Nd^{3+} -ions. All ions within a distance r of the Nd^{3+} -ions are included in the summation (3.26). We can note the large difference in the seemingly converged values. However, as pointed out in the previous chapter, the ions would seem to be too mobile. This will, of course influence the crystal field parameters, and the very large fluctuations in $|A_q^{(k)}|^2$ presented in Figure 5.2 may well be exaggerated.

In order to see the effects of crystal-field parameter fluctuations more clearly, Figure 5.3 shows how the energies vary as a function of environment for the multiplets ${}^4\text{I}_{9/2}$ and ${}^4\text{I}_{11/2}$ at 300 K for (a) Nd_2O_3 and (b) $\text{Nd}^{3+}:\text{LiYF}_4$. It is quite clear that these variations must be taken into account when we later construct a polarized absorption spectra for Nd_2O_3 and $\text{Nd}^{3+}:\text{LiYF}_4$.

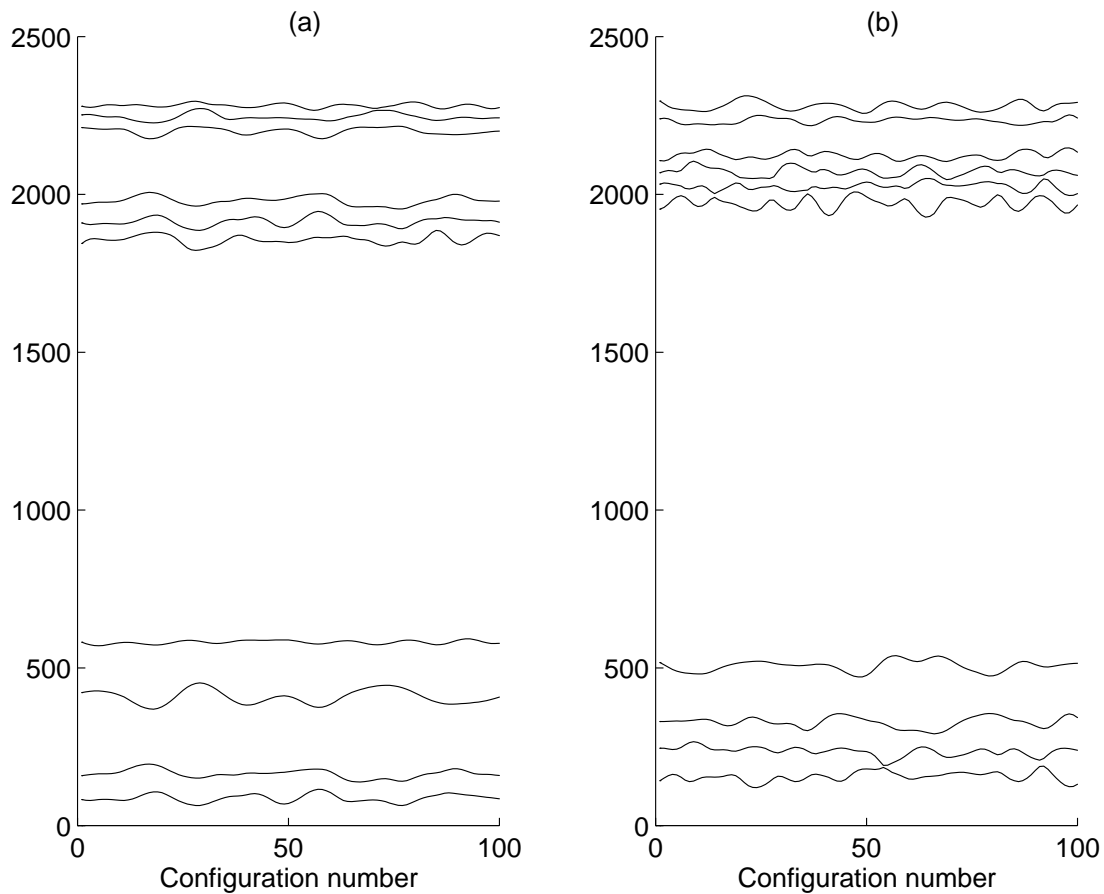


Figure 5.3: The Stark levels (in cm^{-1}) for the two lowest-lying multiplets ${}^4\text{I}_{9/2}$ and ${}^4\text{I}_{11/2}$ are plotted as a function of configuration number. The configurations are in the order generated in the molecular dynamics simulation.

Chapter 6

A structural probe, materials design, laser properties

In this Chapter some ideas will be presented as to how the computational techniques described previously may be applied after further development. There are many areas where access to the enormous amount of information hidden in rare-earth absorption/emission spectrum could be exploited. An understanding of Stark-Stark transition amplitudes and energies is crucial, since these are a function of the crystal field, and therefore a direct fingerprint of the structure surrounding the rare-earth ion. Some parts of the spectrum will depend on the long-range structure and are therefore not directly usable: other parts depend only on the local structure around the rare-earth ion, and it is from these of course in these that the interesting information can be extracted.

That the Stark-Stark transition amplitudes and energies depend strongly on the crystal field should make it possible, in principle, to reverse the calculation and extract local structural information (distances, angles and coordination numbers, etc.) from an absorption/emission spectrum [76]. Similar techniques have been used when fitting the Stark energy levels to experiment [56, 60, 61, 77–84]. However, in their studies a certain local symmetry assumption have been made, implying that only a limited number of the crystal field parameters can be allowed to vary freely in the fitting procedure. Such a technique cannot be applied to the calculation of intensities, because of the large fluctuations in the CF parameters as a result of the thermal motion of the ions (see Chapter 5). Since the calculation of polarized absorption spectra has been shown to be successful for a number of neodymium and erbium compounds, the CF parameters needed to reproduce the experimental spectra are accessible and the local structural information should therefore also be available. This problem has partially been treated by Brawer and Weber [85, 86] and Brecher and Riseberg [87] with respect to the local structure in glasses.

The only problem which arises in using this approach as a “structural probe” is the simulation of the long-range crystal field needed to construct the energy matrix. Although certain parts of the spectrum are characterized by the crystal field resulting from the local structure some realistic model must be assumed to represent the remainder of the structure. If the long-range crystal field is incorrectly described, certain eigenstates will acquire incorrect energies which then interfere with those parts of the spectra which depend only on the local crystal field. It is an insuperable task to distinguish between the transitions which depends on the local structure and the superimposed transitions which have contributions from the long-range crystal field. It is possible that the problem can be partly overcome by

constructing some intermediate to long-range average model structure.

Let us examine, for example, the case of $\text{Nd}^{3+}:\text{LiYF}_4$. "Local structure" can generally be treated viewed as a superpositions of the most common coordination polyhedra; each appropriately distorted and with different r . In LiYF_4 the Nd^{3+} -ion "sees", for example, two tetrahedra rotated $\frac{\pi}{2}$ with respect to one another and with r_1 slightly larger than r_2 ($r_1 = 2.297\text{\AA}$ and $r_2 = 2.244\text{\AA}$). If the absorption spectrum were calculated for this nine-ion cluster (see Figure 6.1), the resulting polarized absorption spectrum bears no likeness to seem to what is observed experimentally. This is because the long-range crystal field has been treated completely incorrectly (not treated at all!). With an incorrect energy matrix, incorrect eigenstates and energies will be the result. Is there some strategy by which we can access this structural information?

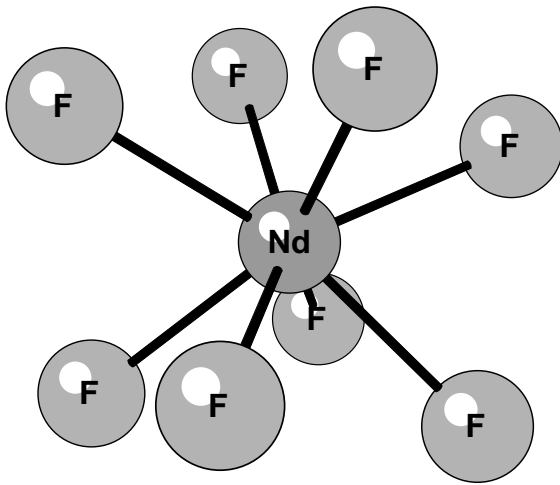


Figure 6.1: The local environment around neodymium in $\text{Nd}^{3+}:\text{LiYF}_4$, see Garcia and Ryan [88]. The two tetrahedra are rotated $\frac{\pi}{2}$ with respect to one another and with r_1 slightly larger than r_2 ($r_1 = 2.297\text{\AA}$ and $r_2 = 2.244\text{\AA}$).

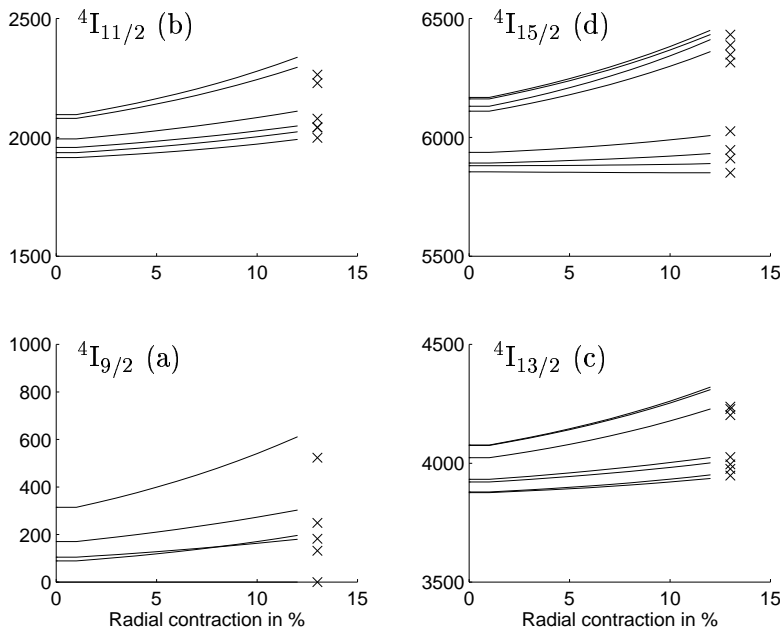


Figure 6.2: The calculated Stark levels (solid lines) for the four lowest lying multiplets of Nd^{3+} in LiYF_4 : ${}^4\text{I}_{9/2}$, ${}^4\text{I}_{11/2}$, ${}^4\text{I}_{13/2}$ and ${}^4\text{I}_{15/2}$ (a-d) plotted as a function of radial contraction from the experimental geometry; the crosses (x) represent the experimental energy levels; see Gama *et al.* [82].

This sensitive influence of "structure" on the calculation described so far can be best illustrated through some examples. Figure 6.2 shows the Stark energies [cm^{-1}] for the lower multiplets ($^4I_{9/2}$, $^4I_{11/2}$, $^4I_{13/2}$ and $^4I_{15/2}$) plotted as a function of radial contraction from the experimental geometry of $Nd^{3+}:LiYF_4$.

Similarly, Figure 6.3 shows the contributions from Er^{3+} -ions ($Er^{3+}:Y_2O_3$) in C_2 - and C_{3i} -symmetry sites. We see clearly the importance of taking the thermally induced motion of the ions into account (paper **V**). The contribution from Er^{3+} -ions in C_{3i} -symmetry sites is certainly not negligible, especially around 300nm and 380nm.

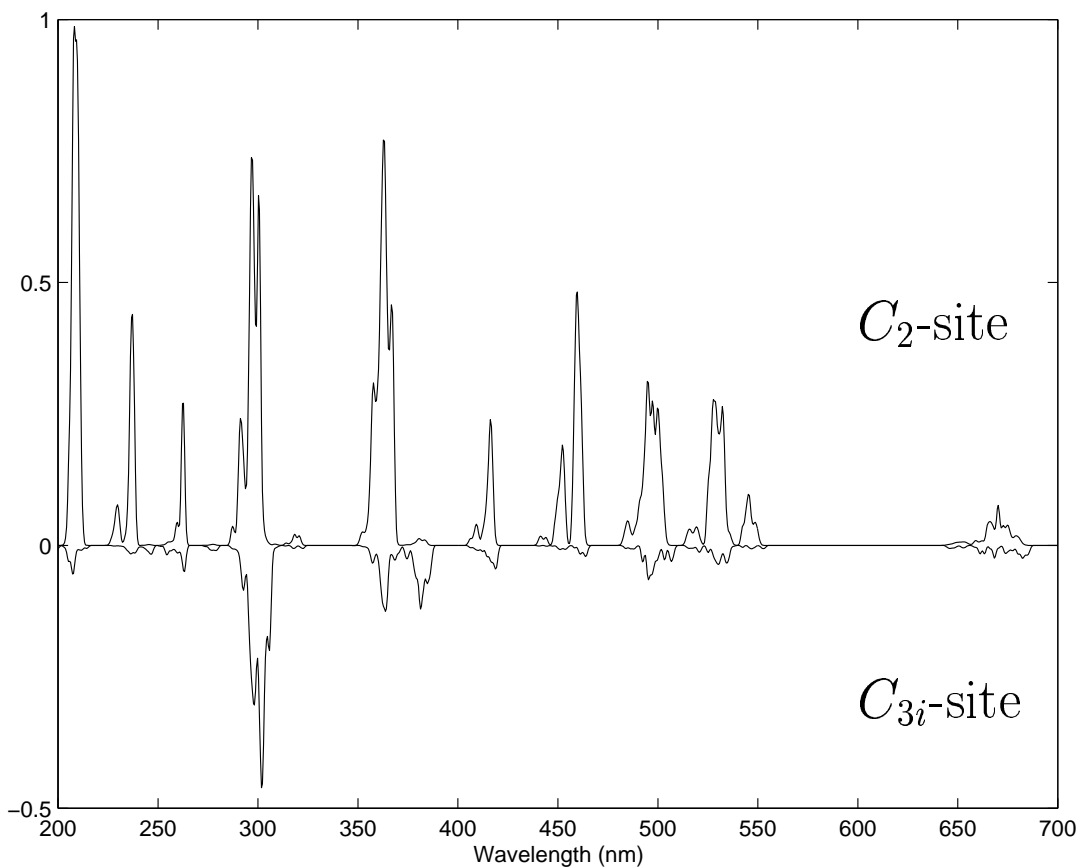


Figure 6.3: The calculated absorption spectrum for $Er^{3+}:Y_2O_3$ in which the contributions from Er^{3+} -ions in C_2 -symmetry sites are plotted above the line, and from Er^{3+} -ions in C_{3i} -symmetry sites below the line, respectively.

A complete procedure for solving the problem illustrated here still lies some time ahead. The problem is by no means unsolvable, but requires computational capability not yet within our reach. However, when solved it will not only be possible to extract local structural information for materials containing rare-earth ions (including amorphous polymers and glasses), it can also be used as a tool for designing materials with some desired optical property (expressed in terms of its absorption/emission spectrum).

A third area of application would be the prediction of laser properties for potential host

materials. For this we would need the calculated polarized emission spectrum. A scheme for calculating such a spectrum is outlined in Section 4.3. The radiative life-time (τ) is given directly by the inverse of the oscillator strength and is therefore readily derivable.

A more delicate problem would be the calculation of the stimulated emission cross-section:

$$\sigma \propto \frac{S(if)}{\Delta\lambda} \quad (6.1)$$

where $S(if)$ is the transition strength and $\Delta\lambda$ is the linewidth. The transition strength is obtained directly given from the calculated oscillator strengths. The linewidth is, in principle, extractable from the MD treatment but will be sensitive to the potential used [Eq. (5.2)], and these were only fitted to reproduce the crystal structure; a many-body potential derived from an *ab initio* treatment would, of course, be preferable. The standard method for calculating the stimulated emission cross-section [Eq. (6.1)] has been to use Judd-Ofelt theory to derive $S(if)$. However, this only gives the oscillator strengths between J -manifolds; current work has improved this type of calculations.

Yet another and possibly even more interesting application of the simulation technique outlined herein is the calculation of branching ratios (β). This branching ratio is a measure of the percentage of emission for given transition from a state i with respect to all other transitions from this state, i.e. summation over the final state j :

$$\beta_{ij} \propto \frac{S(ij)}{\sum_j S(ij)} \quad (6.2)$$

Since, in this thesis treatment $S(ij)$ has been refined (compared to the Judd-Ofelt theory) to give the individual Stark level transitions, we are no longer limited to considering i and j as J -manifolds, but now as individual Stark levels. It should, in principle, be possible to predict the type of structure a potential host-material should have in order to deliver the required branching ratios.

It is important to note at this point that these calculations and predictions are only valid within the approximations made in the applied model; the most severe of these is the use of an electrostatic multipole expansion for the rare-earth environment. This approximation is considered by many to be a gross oversimplification. We have shown it to be valid and sufficient for the compounds investigated here.

Returning to the question implied by the title of the thesis “Rare-earth polarized absorption spectra as a structural tool” (?): it has been shown convincingly that the ground has now been laid for the evolvement of an exciting method in which the power of modern computers combined with the intrinsic accuracy of modern optical spectroscopy to create a valuable “structural tool”.

Chapter 7

Brief summary of results and concluding remarks

It has been demonstrated that polarized absorption spectra can be simulated for a number of rare-earth doped compounds (papers **I**, **II**, **IV**, **V** and **VI**). The key to this has been the use of molecular dynamics together with Racah algebra and the theoretical framework for rare-earth energy levels developed by Rajnak, Wybourne, Judd, etc. This theoretical framework has been merged with a molecular dynamics simulation technique to provide a procedure capable of reproducing experimental polarized absorption spectra.

It has been found that the free-ion CI parameters fitted to reproduce experimental energy levels will also yield good eigenvectors when the energy matrix has been diagonalized. The CI parameters have been shown to be crucial to the success of the method (paper **IV**).

The MD based approach has made it possible to show that sometimes a large error is made if only crystallographically determined positions are used to calculate the crystal-field parameters needed for the intensity simulation. The many different local environments experienced by the rare-earth ions are shown to induce very large fluctuations in the crystal-field parameters. It has also been shown that, for some transitions, it is not possible to ignore contributions from ions located at inversion centres. Thermal motion breaks this inversion symmetry, thus allowing the dipole transitions (paper **V**).

Since the shielding parameters, σ_k , are critical, the Sternheimer method have been used to calculate σ_k for the whole series of rare earths using relativistic wavefunctions. The different $\langle r^k \rangle$ integrals were evaluated in the same paper (**III**).

In contrast with the ideas of many in this field, it is thought that the electrostatic model used in the multipole expansion of the rare-earth ion environment involves no gross oversimplification. The use of an electrostatic model within an MD approach should be examined fully before invoking the more “sophisticated” crystal-field models.

A scheme for calculating polarized emission spectra is proposed. Also, the idea of ‘reversing’ the simulation to gain information about the local structure surrounding the rare-earth ions is put forward. A number of potential areas of application for the simulation technique are also suggested.

The possible sources of error in the simulation technique outlined are:

- a) The MD potential parameters are inadequate since they have only been fitted to reproduce the crystal structures. Moreover we have only used pair potentials; inclusion of appropriate Debye-Waller factors would improve the MD parameters, since these include information about the dynamics of the system.
- b) Uncertainties in the crystal-field parameters $A_q^{(k)}$ through neglect of the effects of covalency and the Ewald summations for $k=1,2,3$.
- c) Correlated crystal-field effects are not considered.
- d) Uncertainties in the matrix element of the different tensor operators which arise from errors in F^k , ζ and the CI parameters.
- e) The problem of labelling eigenvectors; labelling of the high-energy states is difficult, since the eigenstates are a mixture of many ($WUSLJM_J$)-states.

The major advantages of the simulation technique outlined here are:

- a) The calculated absorption/emission spectra are related directly to the structure of the solid/liquid/amorphous material investigated.
- b) The simulation technique is general and can be applied equally well to solid, liquid and amorphous materials.
- c) Since all computer code has been implemented locally, changes and improvements can easily be tested.
- d) Temperature dependence can be treated explicitly.

Future work:

A number of clear routes for further development can be envisaged:

- Polarized emission spectra can be calculated.
- The range of usefulness of the method as a "structural probe" should be investigated further.
- Both CI parameters and Slater integrals are to be evaluated from first principles. This cannot be done today through the inaccuracy of the radial wavefunctions available.
- Computer-aided design of optical materials.

Appendix A

Some useful relations

There now follows a collection of relations that have been used throughout in the text.

A.1 Miscellaneous

Unitary operator:

$$\mathbf{1} = \sum_{\gamma'n'l'm'_i} |\gamma'n'l'm'_i\rangle \langle \gamma'n'l'm'_i| \quad (\text{A.1})$$

The Wigner-Eckart theorem:

$$\begin{aligned} \langle \gamma'n'l'm'_i | T_q^{(k)} | \gamma n l m_i \rangle &= (-1)^{l'-m'_i} \begin{pmatrix} l' & k & l \\ -m'_i & q & m_i \end{pmatrix} \\ &\times \langle \gamma'n'l' || T^{(k)} || \gamma n l \rangle \end{aligned} \quad (\text{A.2})$$

A.2 $n - j$ symbols

The $3j$ -symbols have the following relation to the Clebsch-Gordan coefficients:

$$\langle j_1 j_2 m_1 m_2 | j_1 j_2 j m \rangle = (-1)^{-j_1+j_2-m} [j]^{1/2} \begin{pmatrix} j_1 & j_2 & j \\ m_1 & m_2 & -m \end{pmatrix} \quad (\text{A.3})$$

and the $6j$ -symbol is defined through:

$$\begin{aligned} \left\{ \begin{matrix} j_1 & j_2 & j_3 \\ j_4 & j_5 & j_6 \end{matrix} \right\} &= \sum_{\text{all } m} (-1)^{j_4+j_5+j_6+m_4+m_5+m_6} \begin{pmatrix} j_1 & j_2 & j_3 \\ m_1 & m_2 & m_3 \end{pmatrix} \\ &\times \begin{pmatrix} j_1 & j_5 & j_6 \\ m_1 & m_5 & -m_6 \end{pmatrix} \begin{pmatrix} j_4 & j_2 & j_6 \\ -m_4 & m_2 & m_6 \end{pmatrix} \begin{pmatrix} j_4 & j_5 & j_3 \\ m_4 & -m_5 & m_3 \end{pmatrix} \end{aligned} \quad (\text{A.4})$$

Orthogonality relations:

$$\sum_{j_3 m_3} [j_3] \begin{pmatrix} j_1 & j_2 & j_3 \\ m_1 & m_2 & m_3 \end{pmatrix} \begin{pmatrix} j_1 & j_2 & j_3 \\ m'_1 & m'_2 & m_3 \end{pmatrix} = \delta_{m_1 m'_1} \delta_{m_2 m'_2} \quad (\text{A.5})$$

$$\sum_{m_1 m_2} \begin{pmatrix} j_1 & j_2 & j_3 \\ m_1 & m_2 & m_3 \end{pmatrix} \begin{pmatrix} j_1 & j_2 & j'_3 \\ m_1 & m_2 & m'_3 \end{pmatrix} = \frac{1}{[j_3]} \delta_{j_3 j'_3} \delta_{m_3 m'_3} \quad (\text{A.6})$$

The sum of the products of three $3j$ symbols:

$$\begin{aligned} \left\{ \begin{matrix} j_1 & j_2 & j_3 \\ l_1 & l_2 & l_3 \end{matrix} \right\} \begin{pmatrix} j_1 & j_2 & j_3 \\ m_1 & m_2 & m_3 \end{pmatrix} &= \sum_{\mu_1 \mu_2 \mu_3} (-1)^{l_1 + l_2 + l_3 + \mu_1 + \mu_2 + \mu_3} \\ &\times \begin{pmatrix} j_1 & l_2 & l_3 \\ m_1 & \mu_2 & -\mu_3 \end{pmatrix} \begin{pmatrix} l_1 & j_2 & l_3 \\ -\mu_1 & m_2 & \mu_3 \end{pmatrix} \begin{pmatrix} l_1 & l_2 & j_3 \\ \mu_1 & -\mu_2 & m_3 \end{pmatrix} \end{aligned} \quad (\text{A.7})$$

The $3j$ -symbols possess a number of symmetry relations. For example an odd number of permutations among the columns alter the phase by $(-1)^{j_1 + j_2 + j_3}$. An even number of permutations leave the phase unchanged. Example of the first case:

$$\begin{pmatrix} j_1 & j_2 & j_3 \\ m_1 & m_2 & m_3 \end{pmatrix} = (-1)^{j_1 + j_2 + j_3} \begin{pmatrix} j_2 & j_1 & j_3 \\ m_2 & m_1 & m_3 \end{pmatrix} \quad (\text{A.8})$$

Changing the signs of the magnetic quantum number gives:

$$\begin{pmatrix} j_1 & j_2 & j_3 \\ m_1 & m_2 & m_3 \end{pmatrix} = (-1)^{j_1 + j_2 + j_3} \begin{pmatrix} j_1 & j_2 & j_3 \\ -m_1 & -m_2 & -m_3 \end{pmatrix} \quad (\text{A.9})$$

The $6j$ -symbols remains invariant under any permutation of columns and under transposition of rows in each of any two arguments:

$$\left\{ \begin{matrix} j_1 & j_2 & j_3 \\ l_1 & l_2 & l_3 \end{matrix} \right\} = \left\{ \begin{matrix} j_2 & j_1 & j_3 \\ l_2 & l_1 & l_3 \end{matrix} \right\} \quad (\text{A.10})$$

$$\left\{ \begin{matrix} j_1 & j_2 & j_3 \\ l_1 & l_2 & l_3 \end{matrix} \right\} = \left\{ \begin{matrix} l_1 & l_2 & j_3 \\ j_1 & j_2 & l_3 \end{matrix} \right\} \quad (\text{A.11})$$

Sum rules for $6j$ -symbols:

$$\sum_j [j][l'] \left\{ \begin{matrix} j_1 & j_2 & j \\ l_1 & l_2 & l \end{matrix} \right\} \left\{ \begin{matrix} j_1 & j_2 & j \\ l_1 & l_2 & l' \end{matrix} \right\} = \delta_{ll'} \quad (\text{A.12})$$

$$\sum_j (-1)^{j+l+l'} [j] \left\{ \begin{matrix} j_1 & j_2 & j \\ l_1 & l_2 & l \end{matrix} \right\} \left\{ \begin{matrix} j_2 & l_1 & j \\ j_1 & l_2 & l' \end{matrix} \right\} = \left\{ \begin{matrix} j_2 & j_1 & j \\ l_1 & l_2 & l \end{matrix} \right\} \quad (\text{A.13})$$

Appendix B

An alternative scheme; the seniority number

Following Judd [31], this scheme gives the set of quantum numbers ($l^n \nu U S L M_S M_L$) (which should be compared to ($l^n W U S L M_S M_L$) in Section (2.2)). This is the more natural approach to the problem of classifying l^n states, since it is the result of studying the commutators of double-tensor operators. This is more natural, since in this scheme, the spin and orbital part are not treated as two separate entities (as is done above). Instead, operators of type $T^{(\kappa k)}$ are used with $(2\kappa + 1)$ spin angular momentum components and $(2k + 1)$ orbital angular momentum components. This double tensor is defined to behave as an irreducible tensor of rank κ with respect to S , and as an irreducible tensor of rank k with respect to L . The different commutator relations used to define the algebra of these double-tensor operators can be derived analogously to single-tensor operator commutation relations in Section (2.2). Starting by defining the reduced matrix elements of a double-tensor operator by:

$$\langle n' s' l' || w^{(\kappa k)} || n s l \rangle = \delta_{n' n} \delta_{s' s} \delta_{l' l} \quad (\text{B.1})$$

leads to the following definition of the commutation relations for double-tensor operators:

$$[w_{\pi_1 q_1}^{(\kappa_1 k_1)}, w_{\pi_2 q_2}^{(\kappa_2 k_2)}] = c_{\mu\sigma\nu\rho}^{\lambda\tau} w_{\pi_3 q_3}^{(\kappa_3 k_3)} \quad (\text{B.2})$$

with the structure constants $[\mu = (\kappa_1 \pi_1), \nu = (\kappa_2 \pi_2), \lambda = (\kappa_3 \pi_3), \sigma = (k_1 q_1), \rho = (k_2 q_2)$ and $\tau = (k_3 q_3)$]:

$$c_{\mu\sigma\nu\rho}^{\lambda\tau} = \sum_{\kappa_3 k_3 \pi_3 q_3} [k_3] (-1)^{2s+2l-\pi_3-q_3} \{ (-1)^{\kappa_1+\kappa_2+\kappa_3+k_1+k_2+k_3} - 1 \} \\ \times \left\{ \begin{array}{ccc} \kappa_1 & \kappa_2 & \kappa_3 \\ s & s & s \end{array} \right\} \left\{ \begin{array}{ccc} k_1 & k_2 & k_3 \\ l & l & l \end{array} \right\} \begin{pmatrix} \kappa_1 & \kappa_2 & \kappa_3 \\ \pi_1 & \pi_2 & -\pi_3 \end{pmatrix} \begin{pmatrix} k_1 & k_2 & k_3 \\ q_1 & q_2 & -q_3 \end{pmatrix} \quad (\text{B.3})$$

Since $w_{\pi q}^{(\kappa k)}$ satisfy Eq. (B.2), they can be taken as infinitesimal operators of some groups whose irreducible representations are of interest. Racah [6] and Judd [31] have shown that the following succession of groups and subgroups in $4l+2$ dimensions $[(2l+1)^2(2s+1)^2 = (4l+2)^2]$ is possible:

$$U_{4l+2} \supset SU_{4l+2} \supset SU_{2l+1} \times SU_2 \supset R_{2l+1} \times SU_2 \quad (\text{B.4})$$

Alternatively:

$$U_{4l+2} \supset SU_{4l+2} \supset Sp_{4l+2} \supset R_{2l+1} \times SU_2 \quad (\text{B.5})$$

where Sp is the symplectic group. The representations of SU_2 are defined by the spin multiplicity $2S + 1$. The seniority number (ν) (discussed in great detail in Judd [31]) is defined to be $\nu = \sum \sigma_i$, where $(\sigma_1 \sigma_2 \dots \sigma_{2l+1})$ are the representations of the symplectic group Sp_{4l+2} . When decomposing $Sp_{4l+2} \rightarrow R_{2l+1} \times SU_2$, the irreducible representations of Sp_{4l+2} will thus decompose into the irreducible representations of R_{2l+1} and SU_2 . The branching rules for the case of f^3 are given in Table II (according to Judd [31]).

Table II. $Sp_{4l+2} \rightarrow R_{2l+1} \times SU_2$

ν	$[\sigma_1 \sigma_2 \dots \sigma_7]$	${}^{2S+1}W$
0	(0000000)	${}^1(000)$
1	(1000000)	${}^2(100)$
2	(1100000)	${}^3(110) {}^1(200)$
3	(1110000)	${}^4(111) {}^2(210)$
4	(1111000)	${}^5(111) {}^3(211) {}^1(220)$
5	(1111100)	${}^6(110) {}^4(211) {}^2(221)$
6	(1111110)	${}^7(100) {}^5(210) {}^3(221) {}^1(222)$
7	(1111111)	${}^8(000) {}^6(200) {}^4(220) {}^2(222)$

Since the representations $(w_1 w_2 w_3)$ of R_7 decompose into the irreducible representations L of R_3 , it is seen from Table II that (W) can be dropped and replaced by (νS) . The seniority number indicates in which configuration l^ν the term $({}^{2S+1}L)$ appears for the first time, i.e. it cannot be constructed from $l^{\nu-2}$ by adding the pair l^2 (1S). A Table III corresponding to Table I can now be constructed using this alternative scheme.

The seniority number has been discussed since it enters into the factorization of the fractional parentage coefficients.

Table III. Quantum numbers for f^3

S	ν	$(u_1 u_2)$	L
3/2	3	(00)	S
		(10)	F
		(20)	DGI
1/2	1	(10)	F
1/2	3	(11)	PH
		(20)	DGI
		(21)	$DFGHKL$

Appendix C

The coefficients of fractional parentage for f^3

Instead of trying to solve the complicated system of equations (2.23), Racah showed (using lemma (11) of [6]) that the fractional parentage coefficients break up into a number of factors, each depending on fewer variables. This is highly favourable, since these factors can be calculated or tabulated. For the case of f^n , the fractional parentage coefficients factor out to (Eq. (34) of [6]):

$$\begin{aligned} \langle f^{n-1}(W'U'\tau'S'L')fWU\tau SL \mid \mid f^n WU\tau SL \rangle = & \langle f^2\nu'S' + f \mid \mid f^3\nu S \rangle \\ & \times \langle W'U' + f \mid \mid WU \rangle \langle U'\tau'L' + f \mid \mid U\tau L \rangle \end{aligned} \quad (\text{C.1})$$

where ν is the seniority number. As an example, the following fractional parentage coefficient will be calculated $\langle f^2((110)(11)^3P)f(111)(20)^4D \mid \mid f^3(111)(20)^4D \rangle$. From Table II, it is seen that the seniority number corresponding to $(111)(20)^4D$ is $\nu = 3$ and to $(110)(11)^3P$ is $\nu' = 2$. Racah has given the following formulae (Eq. (52) and Eq. (56) in [6]) for the calculation of the first factor in Eq. (C.1) and its phase $\epsilon \langle \nu'S' \mid \mid \nu S \rangle$.

$$\begin{aligned} \langle l^{n-1}\nu - 1 S - \frac{1}{2} + l \mid \mid l^n\nu S \rangle^2 = & (4l + 4 - n - \nu)(\nu + 2S + 2)S \\ & / [2n(2l + 2 - \nu)(2S + 1)] \end{aligned} \quad (\text{C.2})$$

$$\begin{aligned} \langle l^{n-1}\nu - 1 S + \frac{1}{2} + l \mid \mid l^n\nu S \rangle^2 = & (4l + 4 - n - \nu)(\nu - 2S)(S + 1) \\ & / [2n(2l + 2 - \nu)(2S + 1)] \end{aligned} \quad (\text{C.3})$$

$$\begin{aligned} \langle l^{n-1}\nu + 1 S - \frac{1}{2} + l \mid \mid l^n\nu S \rangle^2 = & (n - \nu)(4l + 6 - \nu + 2S)S \\ & / [2n(2l + 2 - \nu)(2S + 1)] \end{aligned} \quad (\text{C.4})$$

$$\begin{aligned} \langle l^{n-1}\nu + 1 S + \frac{1}{2} + l \mid \mid l^n\nu S \rangle^2 = & (n - \nu)(4l + 4 - \nu - 2S)(S + 1) \\ & / [2n(2l + 2 - \nu)(2S + 1)] \end{aligned} \quad (\text{C.5})$$

and the phase factors:

$$\epsilon \langle \nu'S' \mid \mid \nu S \rangle = (-1)^{S'} \quad \text{for } \nu \text{ odd} \quad (\text{C.6})$$

$$\epsilon \langle \nu' S' \mid \nu S \rangle = (-1)^{S'+(\nu'-\nu)/2} \quad \text{for } \nu \text{ even} \quad (\text{C.7})$$

The second and third factors in Eq. (C.1) are found in Table III and Table IV of Racah [6]. The first factor in Eq. (C.1) becomes, using [Eq. (C.2)]:

$$\langle f^2 \nu' = 2 \ S' = 1 \ + f \mid f^3 \nu = 3 \ S = \frac{3}{2} \rangle = 1$$

The second factor in Eq. (C.1) is:

$$\langle W' = (110) \ U' = (11) \ + f \mid W = (111) \ U = (20) \rangle = -\sqrt{\frac{7}{9}}$$

according to Table III of Racah [6], and the third factor in Eq. (C.1) is:

$$\langle U' = (11)\tau' \ L' = 1 \ + f \mid U = (20)\tau \ L = 2 \rangle = -\sqrt{\frac{27}{49}}$$

according to Table IV of Racah [6]. The phase is given by Eq. (C.6) and $\epsilon \langle \nu' S' \mid \nu S \rangle = -1$. Together, this gives:

$$\langle f^2((110)(11)^3 P) f(111)(20)^4 D \mid f^3(111)(20)^4 D \rangle = -\sqrt{\frac{3}{7}}$$

The remaining coefficients of fractional parentage are derived using this method.

Appendix D

The metric tensor and Casimir's operator

Having derived the expressions for the structure constants [Eq. (2.15) and Eq. (B.3)], the metric tensor (well known from the theory of general relativity) can be expressed for the group in question using the following definition:

$$g_{\sigma\mu} = c_{\sigma\rho}^{\tau} c_{\mu\tau}^{\rho} \quad (\text{D.1})$$

Inserting the structure constants Eq. (2.15) into Eq. (D.1) gives:

$$g_{\sigma\mu} = \sum_{k_2 k_3} [k_2][k_3] (-1)^{q_1} 2 \{1 - (-1)^{k_1 + k_2 k_3}\} \left\{ \begin{matrix} k_1 & k_2 & k_3 \\ l & l & l \end{matrix} \right\}^2 \frac{\delta_{k_1 k_1'} \delta_{q_1 - q_1'}}{[k_1]} \quad (\text{D.2})$$

where Eq. (A.8), Eq. (A.9), Eq. (A.6) and the condition $q_1 + q_2 - q_3 = 0$ have been used. Imposing various restrictions on the right-hand side of Eq. (D.2) makes it possible to describe the metric tensor corresponding to the groups in Eq. (2.17) and Eq. (2.18). Eq. (D.2) is the metric tensor for GL_{2l+1} . According to Judd [31], the following metric tensors are obtained for the groups U_{2l+1} , SU_{2l+1} , R_{2l+1} and G_2 , respectively:

$$g_{\sigma\mu}(U_{2l+1}) = (-1)^{q_1} 2 \{1 - \delta_{k_1 0}\} [l] \frac{\delta_{k_1 k_1'} \delta_{q_1 - q_1'}}{[k_1]} \quad (\text{D.3})$$

$$g_{\sigma\mu}(SU_{2l+1}) = (-1)^{q_1} 2 [l] \frac{\delta_{k_1 k_1'} \delta_{q_1 - q_1'}}{[k_1]} \quad (\text{D.4})$$

$$g_{\sigma\mu}(R_{2l+1}) = (-1)^{q_1} (2l - 1) \frac{\delta_{k_1 k_1'} \delta_{q_1 - q_1'}}{[k_1]} \quad (\text{D.5})$$

$$g_{\sigma\mu}(G_2) = (-1)^{q_1} 4 \frac{\delta_{k_1 k_1'} \delta_{q_1 - q_1'}}{[k_1]} \quad (\text{D.6})$$

Eq.(A.12) and Eq.(A.13) have been used in passing from Eq. (D.2) to Eq. (D.3).

The metric tensor is used in the definition of Casimir's operator for the various groups. This operator will be shown to be very useful for calculating matrix elements for two-particle operators (associated with linear configuration interaction), since its eigenvalues can be calculated. The Casimir operator commutes with all others of the group, and is defined by:

$$G = g^{\sigma\mu} X_{\sigma} X_{\mu} \quad (\text{D.7})$$

$g^{\sigma\mu}$ is related to $g_{\sigma\mu}$ through $g^{\sigma\mu}g_{\sigma\mu} = 1$. The Casimir operators for the group that have been used [$G(U_7)$, $G(SU_7)$, $G(R_7)$, $G(G_2)$ and $G(R_3)$] are given by [using Eq. (D.3) to Eq. (D.6)]:

$$\begin{aligned} G(U_7) &= \sum_{k=0,q}^6 (-1)^q \frac{\{1 - \delta_{k0}\}}{14} [k] U_q^{(k)} U_{-q}^{(k)} = \sum_{k=0}^6 \frac{\{1 - \delta_{k0}\}}{14} [k] (U^{(k)} \cdot U^{(k)}) \\ &= \sum_{k=0}^6 \frac{\{1 - \delta_{k0}\}}{14} [k] (U^{(k)})^2 \end{aligned} \quad (\text{D.8})$$

$$\begin{aligned} G(SU_7) &= \sum_{k=1,q}^6 (-1)^q \frac{1}{14} [k] U_q^{(k)} U_{-q}^{(k)} = \sum_{k=1}^6 \frac{1}{14} [k] (U^{(k)} \cdot U^{(k)}) \\ &= \sum_{k=1}^6 \frac{1}{14} [k] (U^{(k)})^2 \end{aligned} \quad (\text{D.9})$$

$$\begin{aligned} G(R_7) &= \sum_{\text{odd } k=1,q}^6 (-1)^q \frac{1}{5} [k] U_q^{(k)} U_{-q}^{(k)} = \sum_{\text{odd } k=1}^6 \frac{1}{5} [k] (U^{(k)} \cdot U^{(k)}) \\ &= \sum_{\text{odd } k=1}^6 \frac{1}{5} [k] (U^{(k)})^2 \end{aligned} \quad (\text{D.10})$$

$$\begin{aligned} G(G_2) &= \sum_{k=1,5,q} (-1)^q \frac{1}{4} [k] U_q^{(k)} U_{-q}^{(k)} = \frac{1}{4} \{3(U^{(1)} \cdot U^{(1)}) + 11(U^{(5)} \cdot U^{(5)})\} \\ &= \frac{1}{4} \{3(U^{(1)})^2 + 11(U^{(5)})^2\} \end{aligned} \quad (\text{D.11})$$

$$\begin{aligned} G(R_3) &= \sum_{k=1,q} (-1)^q [k] U_q^{(k)} U_{-q}^{(k)} = 3(U^{(1)} \cdot U^{(1)}) = 3(U^{(1)})^2 \\ &= \frac{3}{l(l+1)(2l+1)} \mathbf{L}^2 \end{aligned} \quad (\text{D.12})$$

where the relation $\mathbf{L} = \sqrt{l(l+1)(2l+1)} U^{(1)}$ has been used in Eq. (D.12). The eigenvalues are given by (Racah [6], Judd [31], Edmonds and Flowers [89] and Rajnak and Wybourne [40]):

$$\langle \lambda_1 \lambda_2 \dots \lambda_7 | G(U_7) | \lambda_1 \lambda_2 \dots \lambda_7 \rangle = \frac{1}{28} \sum_{i=1}^7 \lambda_i (\lambda_i + 8 - 2i) \quad (\text{D.13})$$

Note that, for the cases of f^3 and f^{11} , it is not necessary to sum beyond $i = 3$, since $\lambda_i = 0$ for $i > 3$, which can be seen from Table 5-1 in Judd [31].

$$\langle \lambda_1 \lambda_2 \dots \lambda_7 | G(SU_7) | \lambda_1 \lambda_2 \dots \lambda_7 \rangle = \frac{1}{28} \sum_{i=1}^7 \lambda_i (\lambda_i + 8 - 2i) - \frac{n^2}{98} \quad (\text{D.14})$$

$$\langle w_1 w_2 w_3 | G(R_7) | w_1 w_2 w_3 \rangle = \frac{1}{10} [w_1(w_1 + 5) + w_2(w_2 + 3) + w_3(w_3 + 1)] \quad (\text{D.15})$$

$$\langle u_1 u_2 | G(G_2) | u_1 u_2 \rangle = \frac{1}{12} [u_1^2 + u_1 u_2 + u_2^2 + 5u_1 + 4u_2] \quad (\text{D.16})$$

$$\langle LM_L | G(R_3) | LM_L \rangle = \frac{3}{l(l+1)(2l+1)} L(L+1) \quad (\text{D.17})$$

Summary of the papers

- I. Part of the optical absorption spectrum is calculated for the Nd^{3+} -doped $\text{Na}^+ \beta''$ -alumina using a molecular dynamics (MD) based approach. Judd/Ofelt (J/O) theory is modified (and several approximations removed) to treat polarized transition intensities for rare-earth ions in a solid host. It is demonstrated that ions in different local environments contribute differently to the absorption spectrum and, particularly, how the polarization of the various transitions changes for ions occupying different sites.
- II. The complete polarized absorption spectrum is for the first time simulated for the well known laser host material Nd^{3+} :YAG (yttrium aluminium garnet, $\text{Y}_3\text{Al}_5\text{O}_{12}$) using a molecular dynamics (MD) based approach. The theory is presented in detail.
- III. The Sternheimer method is used to derive shielding parameters for the whole series of rare earths using relativistic wavefunctions. It is found that the shielding parameter σ_2 of the 4f electronic shell is decreased compared to earlier calculations.
- IV. It is shown that inclusion of linear and non-linear configuration interaction (CI) parameters greatly improves the simulated polarized absorption spectra for Nd^{3+} :YAG and Nd^{3+} : LiYF_4 . It is found that the CI parameters fitted to reproduce the Stark energy levels also give good eigenvectors (needed for the intensity calculation). The inhomogeneous dielectric mechanism is compared to the standard dipole mechanism. The theory is presented in detail.
- V. As a consequence of the thermally induced fluctuations of the ions in Er^{3+} : Y_2O_3 , it is shown that the intensity contributions from ions in C_{3i} -sites (a site possessing inversion symmetry in the static case) cannot be discarded. The contributions from the C_2 -sites and C_{3i} -sites are compared.
- VI. Energy levels and complete polarized oscillator strengths were simulated for Nd_2O_3 and Nd^{3+} : LiYF_4 . The simulation was static (no MD simulation performed).
- VII. In performing *ab initio* molecular orbital calculations on crystals, the crystal is usually modelled as a cluster of atoms surrounded by a finite set of point charges. This work presents two methods for determining point charges which accurately reproduce the periodic crystal field in the region of the cluster atoms for any unit cell whose unit-cell parameters are known.

Acknowledgements

I would like to thank my supervisor Prof. Josh Thomas for providing me with the opportunity to work in the fascinating field of rare-earth physics. This work would not have been possible without his enthusiasm, positive criticism, and unfailing support and encouragement.

Many interesting and stimulating discussions with Dr. Sverker Edvardsson have been highly valuable to me and this thesis. I am also grateful to him for helping me to get the opportunity to lecture in mathematics at Mid Sweden University during parts of 1996 and 1997. We have also had a lot of fun, especially in Prague and Paris!

I am grateful to Dr. Marvin Weber and Dr. Stephen Derenzo for giving me the possibility to spend time at Lawrence Berkeley National Laboratory. It was very interesting and most inspiring. I also wish to thank them for the excellent accommodation arrangements at UC Berkeley Faculty Club and Berkeley City Club during my two visits. It was during the late summer evenings overlooking San Francisco and the Golden Gate Bridge that most of this thesis was written.

I want to thank my friends and colleagues at the Inorganic Department and especially Jonas Linde for being a Unix guru. A special thank you to Micael Baudin (though you took the desk by the window), with whom I have shared office, a lot of fun, and many beers. I also wish to thank Barbro Lange for expert secretarial assistance.

Financial support from The Swedish Natural Science Research Council and from The US Office of Naval Research is hereby acknowledged.

I wish to thank my parents, my sister (and her family) and all my friends for the support and encouragement they have given me.

Finally, there is Rebecka (tack gumman!), you made it all worthwhile.

Uppsala, September 1997

Bibliography

- [1] M. J. Weber, *The role of lanthanides in optical materials*, Lawrence Berkeley National Laboratory, University of California, Report LBL-37536, UC-404, 1995; (invited) in *Synthesis and Applications of Lanthanide Doped Materials*, American Ceramics Society (1995), pp. 3-20.
- [2] A. A. Kaminskii, *Crystalline lasers: physical processes and operating schemes* (CPC Press, New York, 1996).
- [3] G. Racah, Phys. Rev. **61**, 186 (1942).
- [4] G. Racah, Phys. Rev. **62**, 438 (1942).
- [5] G. Racah, Phys. Rev. **63**, 367 (1943).
- [6] G. Racah, Phys. Rev. **76**, 1352 (1949).
- [7] Slater, Phys. Rev. **34**, 1293 (1929).
- [8] B. R. Judd, Phys. Rev. **127**, 750 (1962).
- [9] G. S. Ofelt, J. Chem. Phys. **37**, 511 (1962).
- [10] I. Lindgren and E. Karlsson, *Tensoroperatorer* (Universitetsförlaget, Uppsala, 1966).
- [11] I. Lindgren, *Atomfysik* (Universitetsförlaget, Uppsala, 1967).
- [12] B. G. Wybourne, *Spectroscopic properties of rare earths* (John Wiley & Sons, New York, 1965).
- [13] B. G. Wybourne, *Symmetry principles and atomic spectroscopy* (John-Wiley & Sons, New York, 1970).
- [14] C. J. Eliezer, *Introduction to selected topics in Lie symmetries* (Matscience report 109, Lawrence Berkeley National Laboratory, University of California, Berkeley).
- [15] G. F. Koster, *Notes on group theory* (Solid-state and molecular theory group, M.I.T., Cambridge, Massachusetts, 1956).
- [16] C. W. Nielson and G. F. Koster, *Spectroscopic coefficients for the p^n , d^n and f^n configurations* (Cambridge, Mass., M.I.T. Press).
- [17] B. R. Judd, *Selection rules within atomic shells*, *Advances in atomic and molecular physics*, **7**, 251 (1971).

-
- [18] B. R. Judd, *Group theory in atomic spectroscopy*, Group theory and its applications, 183 (1968).
- [19] B. R. Judd, *Complex atomic spectra*, Reports on Progress in Physics, **48**, 907 (1985).
- [20] B. R. Judd, *Second quantization and atomic spectroscopy*, Lawrence Radiation Laboratory, University of California, Berkeley, UCRL-16098, 1965.
- [21] D. J. Newman, *Theory of lanthanide crystal fields*, Advances in Physics, **20**, 197 (1971).
- [22] Z. B. Goldschmidt, *Handbook on the Physics and Chemistry of Rare Earths 1, 1 (1978)*, Amsterdam, Netherlands.
- [23] S. Hübner, *Optical spectra of transparent rare earth compounds* (Academic press, London, 1978).
- [24] R. K. Wangsness. *Electromagnetic fields* (John Wiley & Sons, New York, 1986).
- [25] W. K. H. Panofsky and M. Phillips, *Classical electricity and magnetism* (Addison-Wesley, Reading, 1962).
- [26] I. I. Sobelman, *Atomic spectra and radiative transitions* (Springer-Verlag, New York, 1979).
- [27] E. U. Condon and G. H. Shortley, *The theory of atomic spectra* (Cambridge university press, London, 1935).
- [28] J. J. Sakurai, *Modern quantum mechanics* (Addison-Wesley, Redwood City, 1985).
- [29] H. Goldstein, *Classical mechanics* (Addison-Wesley, Reading, 1980).
- [30] M. Jääskeläinen, private communication.
- [31] B. R. Judd, *Operator Techniques in Atomic Spectroscopy* (McGraw-Hill, New York, 1963).
- [32] G. Racah, *Springer Tracts in Modern Physics* (Springer, 1965), Vol. 37, p. 28 .The text is based on a series of seminar lectures at the Institute for Advanced Study, Princeton (1951).
- [33] J. D. Bjorken and S. D. Drell, *Relativistic quantum mechanics* (McGraw-Hill, New York, 1964).
- [34] R. F. Bacher, Phys. Rev. B **46**, 948 (1943).
- [35] R. E. Trees, Phys. Rev. **83**, 756 (1951).
- [36] R. E. Trees, Phys. Rev. **84**, 1089 (1951).
- [37] R. E. Trees, Phys. Rev. **85**, 382 (1952).
- [38] R. E. Trees and C. K. Jørgensen, Phys. Rev. **123**, 1278 (1961).
- [39] G. Racah, Phys. Rev. **85**, 381 (1952).
- [40] K. Rajnak and B. G. Wybourne, Phys. Rev. **132**, 280 (1963).

- [41] K. Rajnak, Phys. Rev. J. Opt. Soc. Am. **55**, 126 (1965).
- [42] B. R. Judd, Phys. Rev. **141**, 4 (1966).
- [43] B. R. Judd, H. M. Crosswhite and H. Crosswhite, Phys. Rev. **169**, 130 (1968).
- [44] B. R. Judd, Proc. Phys. Soc. **82**, 874 (1963).
- [45] K. Rajnak and B. G. Wybourne, J. Chem. Phys. **41**, 565 (1964).
- [46] A. R. Edmonds and B. H. Flowers, Proc. Roy. Soc. A **214**, 515 (1952); J. P. Elliott, B. R. Judd and W. A. Runciman, Proc. Roy. Soc. A **240**, 509 (1957); B. R. Judd, Proc. Roy. Soc. A **250**, 562 (1959).
- [47] B. R. Judd and H. Crosswhite, J. Opt. Soc. Am. B **1**, 255 (1984); H. M. Crosswhite and H. Crosswhite, J. Opt. Soc. Am. B **1**, 246 (1984); B. R. Judd and M. A. Suskin, J. Opt. Soc. Am. B **1**, 261 (1984); J. E. Hansen, P. H. M. Uylings and A. J. J. Raassen, Physica Scripta **37**, 664 (1988); J. E. Hansen and B. R. Judd, Atomic data and nuclear data tables **62**, 1 (1996); B. R. Judd and E. Lo, Atomic data and nuclear data tables **62**, 51 (1996).
- [48] F. A. Parpia, C. Froes-Fischer and I. P. Grant, Compute. Phys. Commun. **94**, 249 (1996).
- [49] D. Garcia and M. Faucher, *Handbook on the Physics and Chemistry of Rare Earths 21, 263 (1995), Elsevier Science B.V.*
- [50] D. J. Newman and B. Ng, Rep. Prog. Phys. **52**, 699 (1989).
- [51] B. Ng and D. J. Newman, J. Chem. Phys. **83**, 1758 (1985).
- [52] B. Ng and D. J. Newman, J. Chem. Phys. **87**, 7096 (1987).
- [53] B. Ng and D. J. Newman, J. Chem. Phys. **87**, 7110 (1987).
- [54] M. F. Reid and B. Ng, Mol. Phys. **67**, 407 (1989).
- [55] G. Burns, J. Chem. Phys. **42**, 377 (1965).
- [56] M. Faucher and D. Garcia, Phys. Rev. B **26**, 5451 (1982).
- [57] P. C. Schmidt, A. Weiss and T. P. Das, Phys. Rev. B **19**, 5525 (1979).
- [58] G. D. Mahan, Phys. Rev. A **22**, 1780 (1980).
- [59] P. Porcher and P. Caro, J. Lumin. **21**, 207 (1980).
- [60] C. A. Morrison, R. P. Leavitt, J. B. Gruber and N. C. Chang, J. Chem. Phys. **79**, 4758 (1983).
- [61] C. Görller-Walrand, L. Fluyt, P. Porcher, A. A. S. Da Gama, G. F. De Sa, W. T. Carnall and G. L. Goodman J. Less Common Metals **148**, 339 (1989).
- [62] O. L. Malta, S. J. L. Ribeiro, M. Faucher and P. Porcher, J. Phys. Chem. Solids **52**, 587 (1991).

- [63] S. Edvardsson, thesis, p. 19-21, Uppsala University, Sweden (1993).
- [64] C. K. Jørgensen and B. R. Judd, *Mol. Phys.* **8**, 281 (1964).
- [65] B. R. Judd, *J. Chem. Phys.* **70**, 4830 (1979).
- [66] M. F. Reid and F. S. Richardsson, *J. Chem. Phys.* **79**, 5735 (1983).
- [67] M. F. Reid, J. J. Dallara and F. S. Richardsson, *J. Chem. Phys.* **79**, 5743 (1983).
- [68] S. Edvardsson, M. Wolf and J. O. Thomas, *Phys. Rev. B* **45**, 10918 (1992).
- [69] J. R. Ryan and R. Beach, *J. Opt. Soc. Am. B* **9**, 1883 (1991).
- [70] M. A. Kramer and R. W. Boyd, *Phys. Rev. B* **23**, 986 (1981).
- [71] M. Wolf, S. Edvardsson and J. O. Thomas, *Phys. Rev. B* **48**, 10129 (1993).
- [72] W. Smith and M. J. Gillan, *J. Phys.: Condensed Matter* **6**, 1319 (1994).
- [73] G. Cormier, J. A. Capobianco, C. A. Morrison and A. Monteil, *Phys. Rev. B* **48**, 16290 (1993).
- [74] G. Cormier, J. A. Capobianco and C. A. Morrison, *J. Chem. Soc. Faraday Trans.* **90**, 755 (1994).
- [75] P. Ewald, *Ann. Phys.* **64**, 253 (1921).
- [76] P. Caro, *J. Alloys Comp.* **193**, 148 (1993).
- [77] C. A. Morrison and R. P. Leavitt, *Handbook on the Physics and Chemistry of Rare Earths 5*, 461 (1982), North-Holland, Amsterdam
- [78] E. Rukmini, A. Renuka Devi, C. K. Jayasankar, *Physica B*, **193**, 166 (1994).
- [79] N. C. Chang, J. B. Gruber, R. P. Leavitt and C. A. Morrison, *J. Chem. Phys.* **76**, 3877 (1982); R. P. Leavitt, J. B. Gruber, N. C. Chang and C. A. Morrison, *J. Chem. Phys.* **76**, 4775 (1982); J. B. Gruber, R. P. Leavitt, C. A. Morrison and N. C. Chang, *J. Chem. Phys.* **82**, 5373 (1985); P. Kisliuk, W. F. Krupke and J. B. Gruber, *J. Chem. Phys.* **40**, 3606 (1964); J. B. Gruber, W. F. Krupke and J. M. Poindexter, *J. Chem. Phys.* **41**, 3363 (1964).
- [80] C. A. Morrison and R. P. Leavitt, *J. Chem. Phys.* **71**, 2366 (1979).
- [81] W. T. Carnall, P. R. Fields and K. Rajnak, *J. Chem. Phys.* **49**, 4424 (1968); W. T. Carnall, P. R. Fields and R. Sarup, *J. Chem. Phys.* **57**, 43 (1972); W. T. Carnall, G. L. Goodman, K. Rajnak and R. S. Rana, *J. Chem. Phys.* **90**, 3443 (1989).
- [82] A. A. S. da Gama, G. F. de Sá, P. Porcher and P. Caro, *J. Chem. Phys.* **75**, 2583 (1981); C. K. Jayasankar, F. S. Richardsson and M. F. Reid, *Inorganica Chimica Acta*, **139**, 287 (1987).
- [83] P. Caro, J. Derouet, L. Beaury and E. Soulie, *J. Chem. Phys.* **70**, 2542 (1979).

-
- [84] G. W. Burdick, C. K. Jayasankar, F. S. Richardson and M. F. Reid, *Phys. Rev. B* **50**, 16309 (1994); J. B. Gruber, J. R. Quagliano, M. F. Reid, F. S. Richardson, M. E. Hills, M. D. Seltzer, S. B. Stevens, C. A. Morrison and T. H. Allik, *Phys. Rev. B* **48**, 15561 (1993); J. B. Gruber, M. E. Hills, T. H. Allik, C. K. Jayasankar, J. R. Quagliano and F. S. Richardson, *Phys. Rev. B* **41**, 7999 (1990); D. Hua, Z. Song, S. Wang and Z. Rong, *J. Chem. Phys.* **89**, 5398 (1988).
- [85] S. A. Brawer and M. J. Weber, *J. Non-Cryst. Solids* **38/39**, 9 (1980).
- [86] M. J. Weber and S. A. Brawer, *J. Non-Cryst. Solids* **52**, 321 (1982).
- [87] C. Brecher and L. A. Riseberg, *Phys. Rev. B* **13**, 81 (1976).
- [88] E. Garcia and R. R. Ryan, *Acta Cryst.* **C49**, 2053 (1993).
- [89] A. R. Edmonds and B. H. Flowers, *Proc. Roy. Soc. A*, **214**, 515 (1952).